Molecular Biology and Evolution, 2025, **42**, 1–19
https://doi.org/10.1093/molbev/msaf187
Advance access publication 7 August 2025
Discoveries

MBE OXFORD

Similar Genetic Routes Are Independently Targeted for Mimetic Color Convergence in Bumble Bees

Heather M. Hines [1,2,*], **Tunc Dabak** [1], **Sarthok Rasique Rahman** [1,3,4], **Tatiana Terranova** [1,5], **Li Tian** [6], **Cecil Smith** [1], **Jonathan Berenguer Uhuad Koch** [7,8], **Jeffrey D. Lozier** [3]

[1]Department of Biology, The Pennsylvania State University, University Park, PA 16802, USA
[2]Department of Entomology, The Pennsylvania State University, University Park, PA 16802, USA
[3]Department of Biological Sciences, The University of Alabama, Tuscaloosa, AL 35407, USA
[4]Department of Ecology and Evolutionary Biology, Princeton University, Princeton, NJ 08544, USA
[5]Department of Molecular Genetics and Microbiology, Duke University, Durham, NC 27710, USA
[6]State Key Laboratory of Agricultural and Forestry Biosecurity, MOA Key Lab of Pest Monitoring and Green Management, Department of Entomology, College of Plant Protection, China Agricultural University, Beijing 100193, China
[7]Pacific Cooperative Studies Unit, University of Hawaii, Manoa, Honolulu, HI 96822, USA
[8]Pollinating Insect Research Unit, U.S. Department of Agriculture - Agricultural Research Service, Logan, UT, USA

***Corresponding author:** E-mail: hmh19@psu.edu.
Associate editor: Aya Takahashi

Abstract

Bumble bees (*Bombus*) exhibit exceptional diversity in setal body color patterns, largely as a result of convergence onto multiple Mullerian mimicry patterns globally. When multiple species cross the same sets of mimicry complexes, they can acquire the same color polymorphisms, providing replicates of phenotypic evolution. This study examines the genetic basis of parallel color pattern acquisition in three bumble bee taxon pairs in western North America that shift between orange-red and black mid-abdominal segmental coloration in Rocky Mountain and Pacific Coastal mimicry regions: polymorphic *Bombus vancouverensis* and *B. melanopygus*, and sister species *B. huntii* and *B. vosnesenskii*. Initial gene targets are identified using a genome-wide association study, while cross-developmental transcriptomics reveals genetic pathways leading to final pigmentation genes. The data show all three lineages independently target the regulatory region of a segmental-fate determining Hox gene, *Abdominal B* (*Abd-B*), for this color transition. For *B. vancouverensis* and *B. melanopygus*, this involves different deletions in the same location, and all mimicry pairs differentially express *Abd-B* and ncRNAs in this locus. Transcriptomics reveals a shared core gene network across species, where *Abd-B* interacts with *nubbin* and pigment enzyme *ebony* to decrease black melanin production in favor of paler, redder morphs. Expression of multiple genes in the melanin biosynthesis pathway is modified to promote this phenotype, with differing roles by taxon. Replicated morphologies unveil key genes and a Hox gene hotspot, while enabling evolutionary tracking of genetic changes to phenotypic changes and informing how gene regulatory networks evolve.

Keywords: Evo-devo, evolutionary genetics, melanin, Hox, ncRNA, convergence

Introduction

Expanding genomic resources have enabled increased understanding of the genetic basis of traits to inform the evolution of phenotypic form. Together, evidence from individual examples can reveal trends in understanding how genotype leads to phenotype, which genes are most important and conserved in imparting phenotypes, and what types of gene regulatory elements and sequences (e.g. *cis* vs. *trans*; Hoekstra and Coyne 2007) are most often modified to impart change. Rapid adaptive radiations offer especially good potential for informing evolutionary genetics, as they lead to exceptional diversity within and between species, but also tend to have multiple examples of convergence that serve as replicates of evolution, making it possible to determine whether the same genes and loci are targeted in parallel under similar selective pressures (Kronforst et al. 2012; Stern 2013; Hines and Rahman 2019).

Systems that engage in Mullerian mimicry, whereby similarly toxic organisms in a region converge on each other's phenotypes to enhance the frequency of warning signals to predators, stand out in revealing these trends. In a model example of Mullerian mimicry, the *Heliconius* butterflies comprise numerous noxious species that have converged on similar wing color patterns within a mimicry zone but diverge in color intraspecifically as they cross mimicry zone boundaries. This creates an ideal framework for uncovering the genetic basis of both traits and convergence, and thus, for decades, these butterflies have served as models for unveiling principles in evolutionary genetics, gene regulation, and evolution (Kronforst and Papa 2015; Merrill et al. 2015; Van Belleghem et al. 2021).

Bumble bees (Hymenoptera: Apidae: *Bombus* Latreille, 1802) are another group of highly color-polymorphic insects that engage in similar Mullerian mimicry. The ~265 bumble bee species distributed across the globe adhere to over 24 regional color pattern-based mimicry complexes (Williams 2007). Many species have a fixed color form that matches their local mimicry complex pattern, but for species with ranges

Received: May 16, 2025. **Revised:** July 9, 2025. **Accepted:** July 21, 2025

that span multiple mimicry complexes, regional color matching produces considerable intraspecific color divergence. As such, phylogenetic mapping of color patterns reveals a radiation of color pattern phenotypes and a scattering of repeated color patterns across the phylogeny (Fig. 1a). This provides an opportunity to understand how similar phenotypes are acquired: this mimicry may be driven by either convergence, ancestral sorting of variation, or adaptive introgression, but determining which requires understanding the genetic basis of these traits.

The colors in bumble bees are imparted in their thick setal dorsal pile and involve combinations of white, yellow, black, and orange-red (referred to as "red" hereafter). These colors tend to be similar across a segment or body sclerite but differ widely in the segmental combinations, with many of the combinations of these patterns by sclerite realized across the 400+ bumble bee color patterns (Williams 2007; Rapti et al. 2014; Fig. 1a). Pigment work across these bumble bees supports yellow setal colors as a likely pterin plus some pheomelanin, white as lacking pigment, black as eumelanin, and red as pheomelanin (Hines 2008b; Hines et al. 2017; Polidori et al. 2017). These setal colors are determined when the primary cuticle of the bumble bee has nearly finished melanizing, with yellow/white versus melanic pigmentation diverging in mid-late pupation, black and red diverging around the onset of adult ecdysis in late pupation (Tian and Hines 2018), and color intensifying rapidly upon adult emergence from the cocoon (Hines et al. 2022).

The *Bombus* mimicry complexes of the western United States present considerable replicates to study the genetic basis of convergence (Fig. 1a). Here, there are two major mimicry patterns – a form with mid-abdominal black coloration in the Pacific region and a form with these same segments red across the Rocky Mountain ecozone. These two mimicry zones share many species that converge onto each local pattern and thus exhibit parallel red–black mid-abdominal polymorphisms (Fig. 1b and c; approximately seven species with polymorphic shifts). These distinct patterns within species are likely a result of historical isolation that generated each color form during glaciation, followed by secondary contact with gene flow (Ezray et al. 2019). Most species that transition between these color forms belong to a fairly closely related clade of bumble bees (*Pyrobombus*), thus offering the potential to track the genetics of these polymorphisms phylogenetically and infer how gene networks generating colors shift over time in acquiring these patterns.

As a foundation for investigating the genetic basis of mimicry in this system, prior research examined the genetic basis of this color dimorphism in one of these species, *Bombus melanopygus*. It is dimorphic with simple Mendelian inheritance (Owen and Plowright 1980) and a narrow transition zone between color forms (Wham et al. 2021). Genomic sampling along this transition zone revealed the genetic basis of this dimorphism to be localized to a 5 kb intergenic region between abdominal Hox genes *Abdominal B* (*Abd-B)* and *abdominal A (abd-A)* (Tian et al. 2019). Hox genes are conserved developmental transcription factors that give distinct fates to different segments of the body by directing a suite of downstream morphology genes in their respective segments. In these bees, this region leads to upregulation in the red morph of *Abd-B*, the Hox gene typically expressed only in the last few "tail" segments of the body, promoting an unusual heterotopic shift of *Abd-B* to more anterior regions of the abdomen. Transcriptome analysis performed in this species at the point of adult eclosion revealed that *Abd-B* generates this color difference by altering the transcription factor (TF) *nubbin* and the pigment gene *ebony*, a melanin enzyme that leads to pale coloration above black pigmentation (Rahman et al. 2021).

Here, we seek to understand how comimics drive their parallel colors by comparing the results of this prior research to the genetic basis of parallel color variation in two additional *Pyrobombus* taxon pairs exhibiting this red–black transition. *Bombus vancouverensis* is an abundant species in the western United States and exhibits a gradual color transition and intermediate color patterns between black forms in Pacific Coastal states and red forms in the Rocky Mountains (Fig. 1; Ezray et al. 2019), thus, color regulation is likely multigenic. Sister lineages *B. bifarius* and *B. ternarius* exhibit red coloration; thus, the black color in *B. vancouverensis* is likely derived (Lozier et al. 2013; Ghisbain et al. 2020). In the second pair, sister species *Bombus huntii* and *Bombus vosnesenskii* adhere to the Rocky Mountain (red) and Pacific Coastal (black) zones, respectively, with each of these species exhibiting fixed coloration. As abundant species representing the most highly fidelity patterns for their respective regions (Fig. 1a), *B. huntii* and *B. vosnesenskii* are likely models for their respective mimicry complexes (Ezray et al. 2019). Assessing the genetic basis of color in this pair is challenging because of their lack of gene flow; nevertheless, we utilize these species to examine sequence variation in genome regions identified in the other mimicking species and to compare patterns of gene expression.

In this study, we test whether the parallel shifts in mimetic color forms across these three comimicking taxon pairs involve the same genes, mutations, and gene networks, and examine how these genes evolve across the mimetic radiation. If all three taxon pairs were to utilize the same variants to generate this variation, a common origin and either ancestral allele sorting or adaptive introgression would be implicated. If different mutations are involved, this would instead suggest convergence. Similar loci could be targeted independently if this was the optimal target to impart change (evolutionary hotspots), or different genes in the gene network leading to pigmentation could be targeted, suggesting diverse potential routes to the same outcome. To determine which is the case, we identify the genetic target driving these color patterns in *B. vancouverensis* using genome-wide association study (GWAS) and compare the locus to *B. melanopygus* and across other closely related *Pyrobombus* species. We also track the evolution of gene expression networks that convert initial mutations to color phenotypes across this radiation by performing transcriptome analysis across the developmental span of this phenotype from late pupation through early adulthood in *B. melanopygus*, *B. vancouverensis*, *Bombus huntii–Bombus vosnesenskii*, and two black form sister lineages. This reveals conserved and variable elements in the gene networks that connect genotype to phenotype. Altogether, these data support a framework for how this color pattern radiation evolved to inform how both diversity and convergence can be generated.

Results

The Genetic Locus for the Mimetic Color Polymorphism

Inheritance and Complexity of Coloration in B. vancouverensis

We assessed heritability and dominance of color variation in *B. vancouverensis* by comparing color phenotypes of the color-variable mid-abdominal (technically metasomal; both

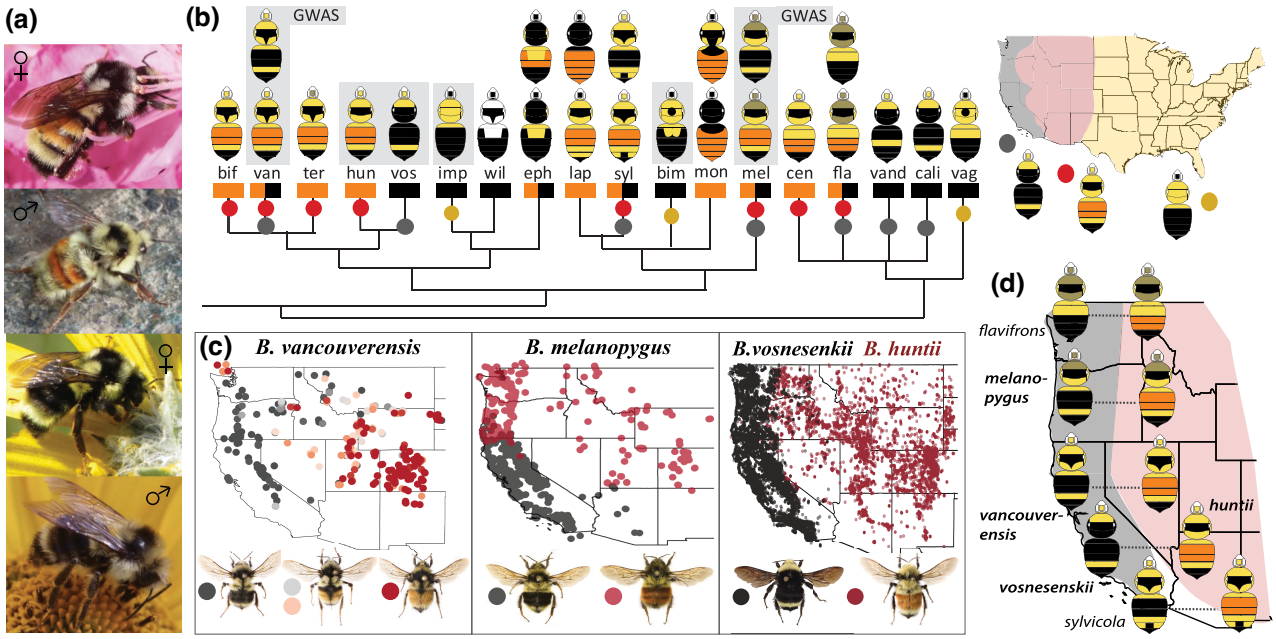

Fig. 1. Evolution of red and black mimetic color polymorphisms in the *Bombus* (*Pyrobombus*) lineage. a) Workers and males of *B. vancouverensis* red and black form. b) The phylogeny of the *Pyrobombus* subclade (based on Hines 2008a) that contains most of the color forms adhering to the mimicry complexes in North America, showing color pattern variation with bee diagrams, the evolution of mid-abdominal red versus black coloration in boxes below bee diagrams, and membership to the three primary mimicry complexes of the United States with colored circles corresponding to the geographic mimicry zones in the map at right. Mimicry zones are defined using specimen color frequencies and machine learning techniques based on Ezray et al. (2019), with the centric color pattern for each region indicated by the color diagram below the map. Species with no colored circle in the phylogeny occur outside of the United States. Species sampled for transcriptomics have their color patterns outlined with gray boxes. Those with "+GWAS" are assessed for their color locus using GWAS. Species names are abbreviated with their first three letters. c) Distribution of red and black color forms of each of the three main lineages studied here. Locality data by phenotype for the polymorphic species *B. vancouverensis* and *B. melanopygus* are modified from Ezray et al. (2019), and the monomorphic *B. huntii* and *B. vosnesenskii* are derived from GBIF records (GBIF, 2025). Intermediacy in color is indicated by intermediate shading for *B. vancouverensis*. d) Schematic of the parallel color transitions between the two major mimicry zones among species in *Pyrobombus*. Figures (b to d) show females, but males have the same pattern for the studied species. Photo credits: iNaturalist CCO from top: selwell, ensrping, and selwell (British Columbia, Canada); swells (Idaho, USA).

terms used interchangeably here) segments (M2 + M3) among queens, workers, and males from 34 colonies reared in common laboratory conditions from wild-caught queens (parental male unknown). Color appears to be heritable, as queen phenotypes that fall across the red to black color gradation match closely with the phenotypes of both their male and female offspring (supplementary fig. S1, Supplementary Material online). The coloration is likely polygenic, given the continuous gradation of phenotypes, but also because hemizygous males exhibit intermediate coloration percentages similar to their mothers. Given the haplodiploid sex determination in bees, if this were a single-locus diallelic trait, the haploid male offspring of diploid heterozygous queens would be dimorphically black or red.

While workers and males tend to be similar by colony, workers in *B. vancouverensis* tend to be slightly more black than males (supplementary fig. S1a and b, Supplementary Material online). We compared the mean percent red (area red/(total area red + black)) of mid-abdominal (M2 + M3) segments for both workers and males in colonies with both sexes, and averaged these means across colonies: workers averaged 33% red and males 52% red (supplementary fig. S1b, Supplementary Material online). A higher frequency of mid-abdominal red in males is also found in field collections from wild populations (supplementary fig. S1c, Supplementary Material online). One explanation for this is that alleles for black coloration are more dominant, which would generate a greater frequency of black forms in females (diploid) than males (haploid). There may also be impacts of sex and caste on phenotype, especially considering that developmental time varies by caste and sex (Plowright and Jay 1977; Tian and Hines 2018).

An Evolutionary Hotspot for Red–Black Polymorphisms

To investigate the genetic basis of color variation in *B. vancouverensis*, we performed a GWAS using whole-genome resequencing of male specimens from wild populations, including 24 individuals that are red and 24 that are black in segments M2 + M3 (Fig. 2a; supplementary table S1, Supplementary Material online). Males were sampled because they are haploid and thus avoid dominance effects and enable improved filters on data quality. Given that *B. vancouverensis* has a gradual cline and full red and full black forms from the transition zone are rare, we were not able to sample from an evenly admixed population (Fig. 2a). The first two PCA axes of these genomic samples (Fig. 2b) explain only 6.2% of the total variation, but show the samples cluster by coloration and geography, indicating the potential for color patterns to be confounded with geographically sorting loci. Most of the separation on these axes, however, is driven by the westernmost black form samples along the Cascade mountains, as red and black individuals from northeastern Oregon and Idaho cluster closely with red individuals from Utah. Despite the potential for geographic signal confounding associations, very few loci had strong associations with color in the GWAS, suggesting that there is considerable gene flow despite some geographic signal in the data.

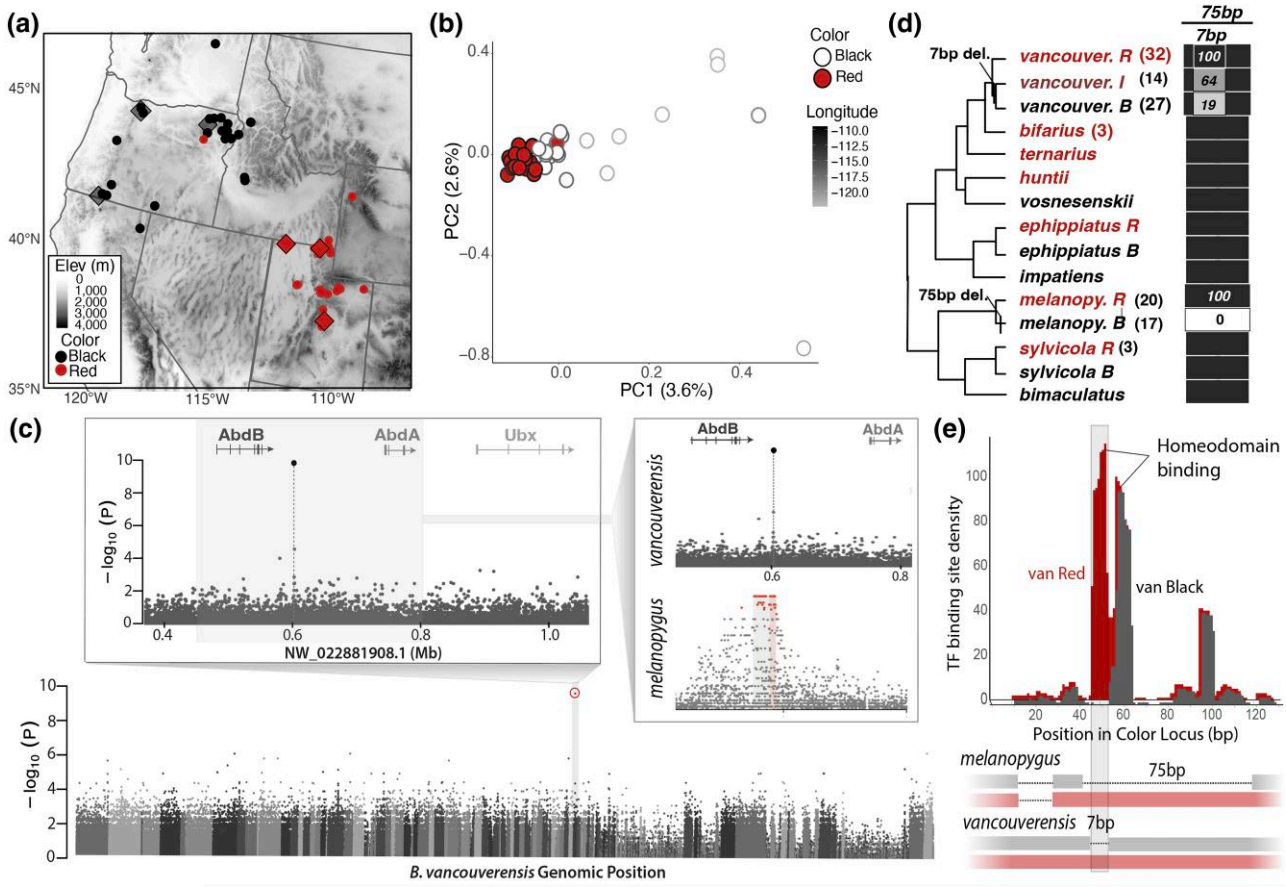

Fig. 2. Patterns of genetic variation and the inferred locus driving color variation in *B. vancouverensis*. a) Distribution of samples used for genomic sequencing (dots) and transcriptomic analysis (diamonds) by color form. Only nearly full red or black samples were included. b) Clustering by genomic variants across each specimen used in the genomic analysis, with fill color reflecting mid-abdominal coloration and fill outline shade reflecting longitude. c) GWAS across the genome for the genomic samples (bottom; most associated variant circled in red) and GWAS of a zoomed region of the genome (above), showing that the most associated indel variant falls in the intergenic region between *Abd-B* and *abd-A*. At right is a comparison of the position of the single indel in *B. vancouverensis* compared with the peak of association driving the same phenotypes in *B. melanopygus* (Tian et al. 2019). For *B. melanopygus*, the gray shaded area (and red colored SNPs) is the block of fixed sites for genomic sequencing, and the red shaded area represents the region that remained fixed after additional Sanger sequencing of individuals. d) Phylogenetic perspective on the origin of each deletion, including its distribution in *B. vancouverensis* relative to color form. R, red form, B, black form, I, intermediate coloration. The number of individuals compared with both Sanger and whole-genome sampling is indicated in parentheses. The block at right indicates the presence and absence of the 7 or 75 bp indels, and the numbers present the percent of samples with the deletion variant (R, red, B, black, I, intermediate). Black bars have no deletions. The phylogeny is based on Hines (2008a). e) Comparison of deletions in *B. melanopygus* and *B. vancouverensis* black form and red forms (bottom) with TF binding site number for each base position indicated for both red and black *B. vancouverensis* sequences.

The GWAS does not show any clear multivariant peaks (Fig. 2c). We instead found just a single variant that fell considerably above the background signal (P-value $= 1.8 \times 10^{-10}$; Benhamini-Hockberg adjusted P-value $= 9.2 \times 10^{-4}$). The associated variant is a 7 bp indel (deletion found in 87.5% of black form and 0% of red form individuals) that falls in the same location as the previously discovered *B. melanopygus* color locus. Notably, the 7 bp *B. vancouverensis* deletion overlaps a 75 bp fixed deletion in *B. melanopygus*, also present only in the black form and absent in all red individuals, that occurs in the center of a 5 kb locus of fixed sites that drive red–black dimorphism in this species. As this is a different deletion, this suggests that each of these lineages has independently targeted this same locus to drive the same color variation (Fig. 2c to e).

As noted above, the deletion in *B. vancouverensis* is not fixed relative to color form. We further examined the presence of this deletion by color form by sequencing additional male (12) and female (4) *B. vancouverensis* across this genetic region using Sanger sequencing. In total, all red forms ($n = 32$) lacked the deletion, while 5 of 27 black form individuals lacked the deletion (Fig. 2d). For black form specimens that deviate from the typical deletion allele, manual inspection of variants and aligned reads revealed that there is no clear variant in neighboring regions or more broadly in the intergenic region between *abd-A* and *Abd-B* that would explain their alternative regulation. Therefore, either another locus operates to generate black color in this species, or there are multiple variants in the region that in combination, can yield this effect. An exploration of reads mapping to the region ±25 kb surrounding the deletion did not support any linked color-associated variants or larger indel variants that were missed with single nucleotide polymorphism (SNP) and indel calling. Linkage disequilibrium (LD) analysis supported very little linkage in this genetic region among sampled *B. vancouverensis*, unlike *B. melanopygus*, which shows considerable linkage blocks, thus suggesting that very high recombination and admixture lead to identification of a single-associated variant (supplementary fig. S2, Supplementary Material online).

The above analyses focused on samples that were selected based on the most extreme red/black phenotypes; however, many *B. vancouverensis* individuals have a more intermediate pigmentation in the M2 + M3 segments. We sequenced males from four of the most color-variable *B. vancouverensis*

colonies and found a weak correlation of the deletion with intercolony color variance, suggesting that intermediacy is influenced by other loci in these colonies (supplementary table S2, Supplementary Material online). We examined the presence and absence of the deletion in genomes of 10 males and 1 female from Utah, with the highest levels of black found in the region (25% to 50% red in mid-abdominal segments); 3 of 11 intermediates had the deletion, while all full red forms from Utah lack the deletion. When including additional Sanger sequenced males from eastern Oregon, 5 of 14 intermediates had the deletion. We compared female genotypes to better understand the dominance effects under diploidy: one red female did not have the deletion, one black female was homozygous for the deletion, and two were heterozygous for the deletion. These data suggest that the deletion generates a darker color when present, but that other unidentified loci are also contributing to the dark color.

Independent Evolution of the Mimetic Color Locus

To examine the phylogenetic history of the deletion locus, we examined a combination of targeted Sanger sequencing and whole-genome sequences (supplementary table S3, Supplementary Material online) in closely related species from the *Pyrobombus* subgenus (most recent common ancestry of ~10 MYA; Hines 2008a) that have either red or black pile on their mid-abdominal segments (supplementary fig. S3, Supplementary Material online). Based on this sequencing, no species except for *B. melanopygus* or *B. vancouverensis* exhibit a deletion in this region, indicating that the ancestral state is to have no deletion in this region (Fig. 2e). Thus, the black forms of both *B. melanopygus* and *B. vancouverensis* appear to have acquired their respective deletions de novo and not from sister taxa. Manual scans across whole-genome alignments of the *Abd-B-Abd-A* intergenic region identified no other obvious variants that segregate with red or black forms across species. Regulation of red and black form phenotypes in other species likely utilizes other species-specific mutations in this intergenic region or occurs elsewhere in the genome. For example, there are no variant bases in the 100 bp surrounding the deletions in the sister taxa *B. huntii* (red) and *B. vosnesenskii* (black), or for red and black mid-abdominal color variants of either *B. sylvicola* or *B. ephippiatus* (Mexican origin; Duennes et al. 2012; supplementary fig. S2, Supplementary Material online).

Functional Features of the Deletion Region

We assessed whether the 7 bp deletion in *B. vancouverensis* impacts TF binding using a JASPAR-based transcription factor binding site (TFBS) prediction analysis. The deletion region is enriched for TFBS, as it contains an AT-rich sequence that is a binding site for many members of the homeobox gene family, including Hox genes, pair rule, and segment polarity patterning genes (JASPAR homeo domain cluster, Fig. 2e). There are two neighboring homeodomain binding sites: the *B. vancouverensis* deletion causes one to be lost, while the *B. melanopygus* deletion causes a loss of both.

Transcriptomics Supports a Core Network Driving the Color Polymorphism

Transcriptome Samples and Their Patterns of Variation

We performed comparative transcriptomics (100 bp paired-end Illumina RNA sequencing) across the three mimicry pairs on epidermal tissue of T2 + T3 metasomal segments from males from three developmental stages spanning the timing of color development. We sampled seven replicates per condition, including *B. melanopygus* red and black form, *B. vancouverensis* red and black form, and *B. huntii* (red form) and *B. vosnesenskii* (black form) ($n = 126$ samples total; supplementary table S4, Supplementary Material online). The earliest developmental stage sampled, pupal stage P15, is when the first indication of color differences in the pale peach setae is apparent (Tian et al. 2019), and thus represents the likely start of differential gene expression. We also sampled both 0 and 12 h post-emergence (adults) from the pupal wax cell/cocoon. At 0 h, melanic red and black colors rapidly increase and 12 h is in the middle of melanin deposition (Hines et al. 2022; Fig. 3c). We sampled quiescent stages for *B. vancouverensis* ($n = 4$/color form), a stage between P15 and 0H where the bee finalizes shedding of pupal cuticle, expands its wings, and that is ~24 h prior to emergence. We also sampled a stage when most melanization is complete 24 h post-eclosion, for both *B. vancouverensis* and *B. melanopygus* ($n = 4$ each). These extra stages were included to more closely examine expression patterns of genes of interest over time. We also included seven replicates each of *Bombus impatiens* (P15, 0, and 12H) and *B. bimaculatus* (P15 and 0H) epidermal tissues, which are black in M2 + M3, to enable a phylogenetic perspective on gene expression.

Clustering analyses of all transcriptomes reveal that the greatest variation in gene expression is related to stage of development, transitioning from P15 to quiescent to early adult stages (Fig. 4a and b). The 0 to 24H adults are partially overlapping with some transitioning in gene expression by age. Very little clustering occurs by species and color (Fig. 3a), indicating that the majority of the transcriptome does not show color-specific gene expression, and developmental transcription in this tissue is conserved across species. These results suggest that the developmental point of sampling of individual bees is a major source of variance.

Differentially Expressed Genes Across Mimicry Pairs

Differential gene expression analysis reveals a set of shared differentially expressed genes (DEGs) across the three mimicry pairs. These are mostly differentially expressed in 0 and 12H stages, with only *Abd-B* being differentially expressed to some degree across all three stages and by all three pairs (Fig. 3d). In P15, there are few shared DEGs across mimicry pairs and fewer DEGs are observed compared with later stages (Fig. 3d; supplementary fig. S4, Supplementary Material online). More genes are shared between 0 and 12H, as may be expected given their temporal proximity and the clustering analysis (Fig. 3d). Although the number of genes upregulated in black versus red forms is proportionally similar across mimicry pairs, DEGs that are shared across species are mostly upregulated in red forms, and these red form upregulated genes tend to have higher fold change and lower *P*-values (Fig. 4d and e; supplementary table S3, Supplementary Material online).

The number of DEGs varied by mimicry pair. The *B. huntii–vosnesenskii* comparison has far more DEGs than the other species, most likely reflecting their distinct species status that produces many inherent differences in gene expression unrelated to color phenotypes. Our exploration of some of these genes showed that differences in splicing of genes and sequence variation also impact coverage. The *B. vancouverensis* individuals sampled came from colonies that were either

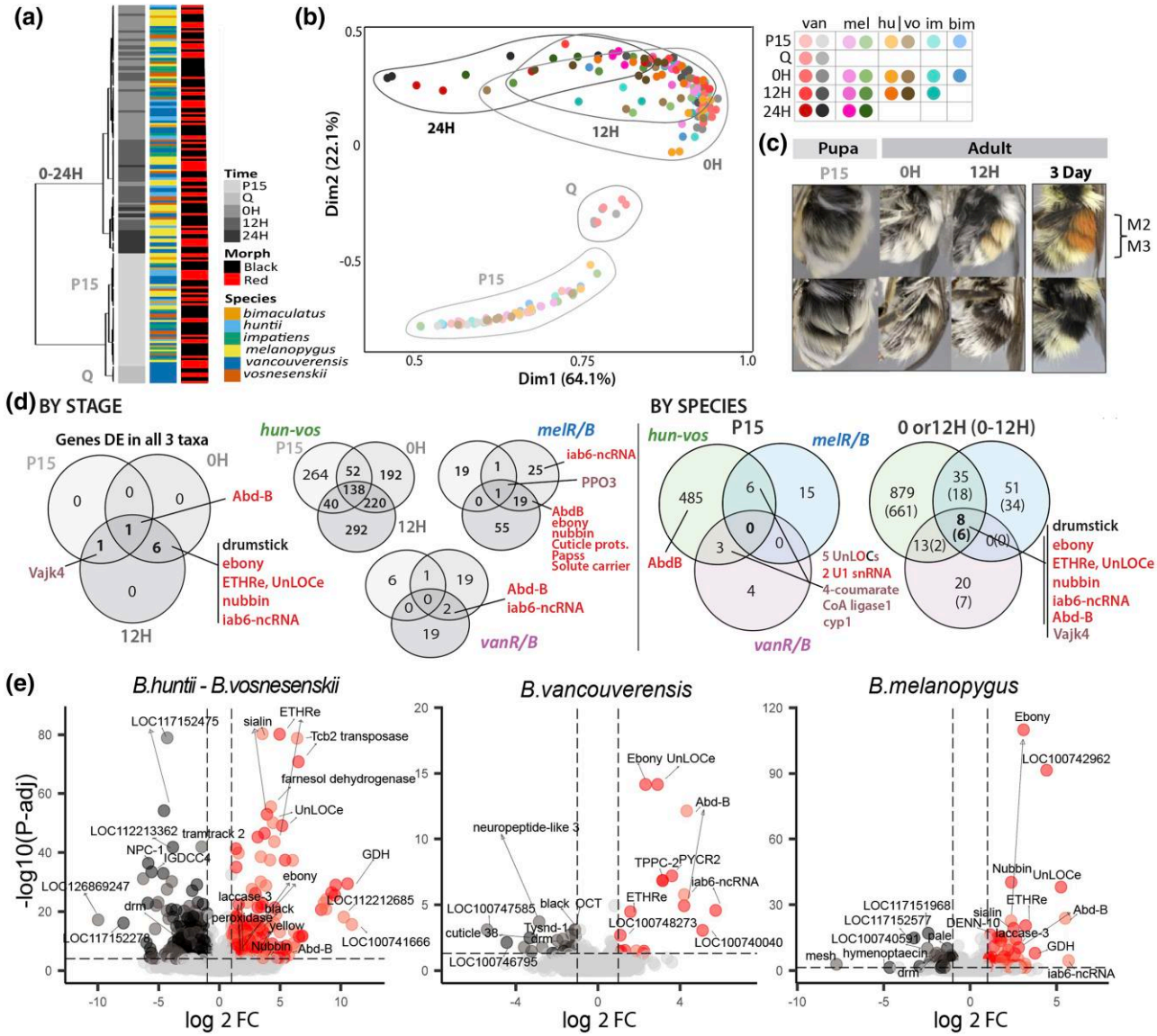

Fig. 3. Patterns of transcriptome variation and shared DEGs across mimicry pairs and stages. a) Relationships between transcriptome samples diagrammed by condition (stage, morph, species). b) Spatial clustering results for samples, showing that the primary clustering is explained mostly by stage. The legend for dot colors is at right with species abbreviated by the first 2 to 3 letters. c) Primary stages sampled in pupae and adults, with the appearance of bee abdomens during these stages for red and black form *B. melanopygus*. Three-day bees were not sampled but are shown to indicate the coloration of a fully pigmented bee. The sampled segments M2 and M3 are indicated. d) Venn diagrams of DEG sets across stages and species. BY STAGE, at left shows only the eight genes differentially expressed in all three taxon pairs, showing the stage combinations in which each of these is represented. Gene names are colored according to the color form in which they have higher expression. The Venn at right is the DEGs by stage for each taxon pair, with the most interesting genes indicated. DE, differentially expressed. BY SPECIES shows the number of DEGs shared by species for each stage. "0 or 12H" gene lists are merged post-analysis and considered present for a species if in lists for either stage. "0 to 12H" samples (results in parentheses in the plot at the right) are from merging the data from these stages before analysis (lines next to names shows the 8 and 6, respectively). e) Volcano plots for the three taxon comparisons at 0 and 12H, with both 0H (lighter colored dots) and 12H (darker colored dots) samples overlaid. Some of the most DEGs are indicated, as well as key melanin and core pathway genes.

>75% red or <25% black in mid-abdominal segments, thus were more intermediate in color than the fully dimorphic *B. melanopygus*. This may explain why *B. vancouverensis* tended to have fewer and less strongly DEGs than *B. melanopygus* (Fig. 3e).

P15 patterns—The only genes with shared differential expression by more than one species in P15 are not obviously relevant to coloration (Fig. 3d; supplementary fig. S4, Supplementary Material online). The first gene targeted for *B. vancouverensis* and *B. melanopygus*—*Abd-B*—was only significantly differentially expressed in P15 in B. *huntii–vosnesenskii* (Fig. 3d). This lends support to this gene being important in early stages for B. *huntii–vosnesenskii* as well. *B. melanopygus* and *B. vancouverensis* did not have significant differences in expression of *Abd-B* in P15, but there were significant differences in qPCR at this stage in *B. melanopygus* in a prior study (Rahman et al. 2021), and their mean expression was significantly higher in red form when *P*-values are not adjusted for multiple comparisons (Fig. 4). As *Abd-B* is beginning to be upregulated at P15, some individuals may not have started this process, thus our P15 data is not expected to provide much valuable information on subsequent genes in the pathway.

0 + 12H—As 0 and 12H stages are very close together, involve deposition of pigments, and yield many shared DEGs

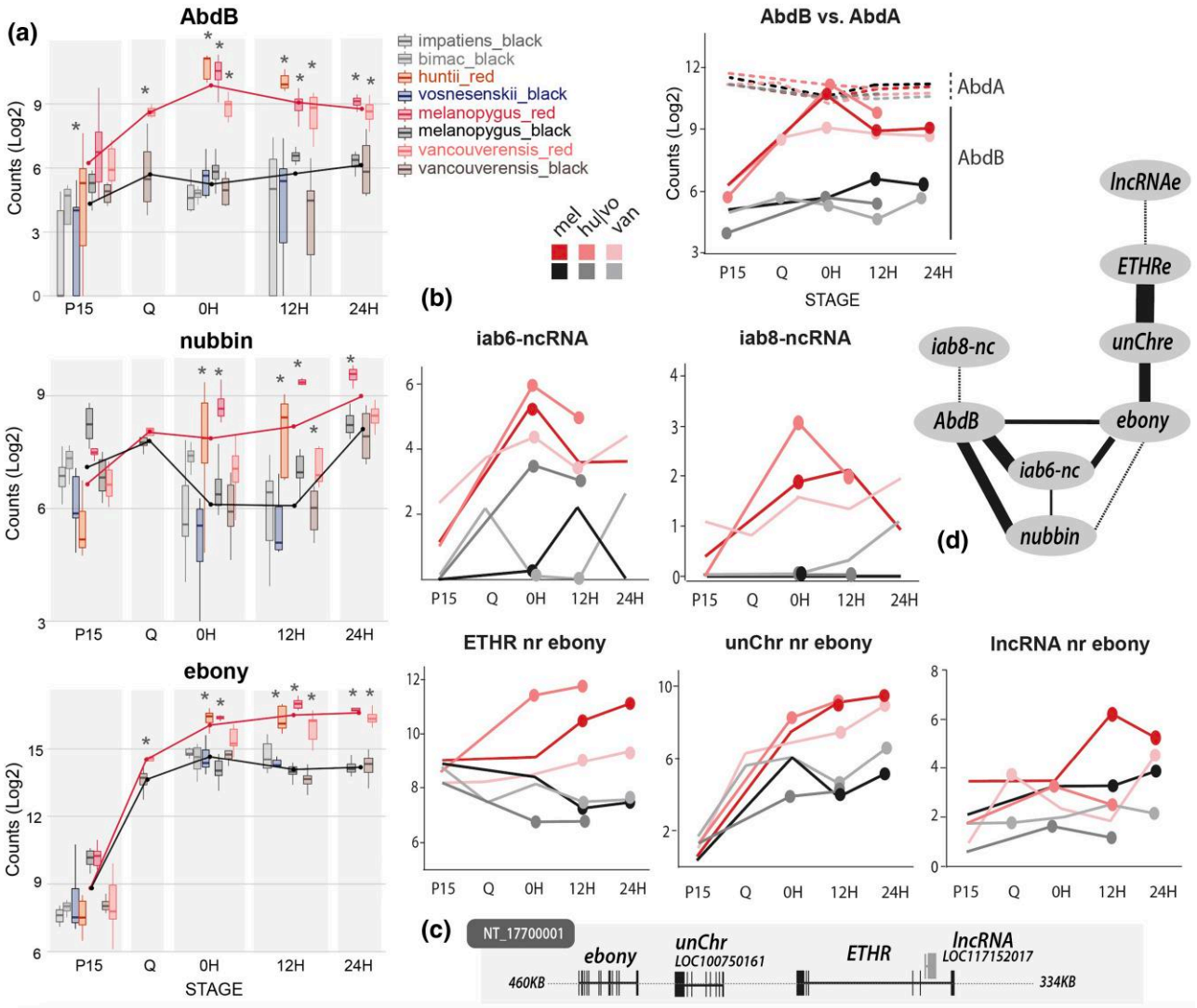

Fig. 4. Differential gene expression of the core set of genes across species and color forms. a) *Abd-B, nubbin,* and *ebony*, as leading genes across all three species, are featured with box plots for each condition, with asterisks indicating differential gene expression. b) For other genes, mean $\log_2$ normalized count values across replicates are shown with circles, indicating differentially expressed comparisons and color shade reflecting different mimicry pairs. Featured are the two lncRNAs in *Abd-B* and the three genes in a linkage group with *ebony*, including ETHR (*ETHRe*), and an uncharacterized protein LOC100750161 (aka. *Thelytoky* in *Apis, unChre*), and a lncRNA in the ETHR gene (LOC117152017; *lncRNAe*). The genomic position of these linked genes is indicated at bottom (c). A comparison of *Abd-B* to Hox gene *abd-A* is also shown. d) An extract of the consensus gene network across 0, 12, 0 + 12, and all combined for *B. melanopygus* and *B. vancouverensis*, showing the linkage of each of these genes. Line thickness reflects the summed weight across each group comparison. Dashed lines are for summed weights that fall below the threshold to show edges in Fig. 5.

between stages, we merged DEG lists for both stages to compare common genes across species. We also ran a differential gene expression analysis merging individuals from both stages to determine which genes remained under increased discriminatory power (supplementary table S5, Supplementary Material online).

The three taxon pairs share a core set of DEGs. In particular, this involves upregulation of *Abd-B* in red forms, followed by upregulation of TF *nubbin* and the melanin pathway enzyme *ebony*. Gene network analysis for *B. vancouverensis* and *B. melanopygus* indicates that these three genes are closely linked, reinforcing their shared connections. The timing of the expression of these core genes across development suggests that *Abd-B* is expressed first, followed by *nubbin* and *ebony*; the network linkages for *Abd-B* with these genes weaken by 12H, and peak differential expression of *Abd-B* is at 0H, while the other two are higher at 12H. The gene network analysis supports that both may be regulated by *Abd-B* or the ncRNAs in the *Abd-B/Abd-A* intergenic region.

The upregulation of *Abd-B* is not mirrored by patterns in *abd-A*, which are stable across this developmental period. *abd-A* has higher expression in this mid-abdominal region than *Abd-B* across much of this time period, as is typical for this Hox gene; however, at adult eclosion, the two reach equal or near-equal levels of expression in red forms only. This shift may impact which protein dominates, as in *Drosophila* embryos, *Abd-B* prevents *abd-A* translation, or lead to more complicated interactions, as these genes work together in more combinatorial ways in embryogenesis of other arthropods (Martin et al. 2016).

Three additional genes are expressed in concert with these core genes: a growth hormone secretagogue gene in *Drosophila* known as ETHR, an uncharacterized locus LOC100750161, and an ncRNA LOC117152017 located in

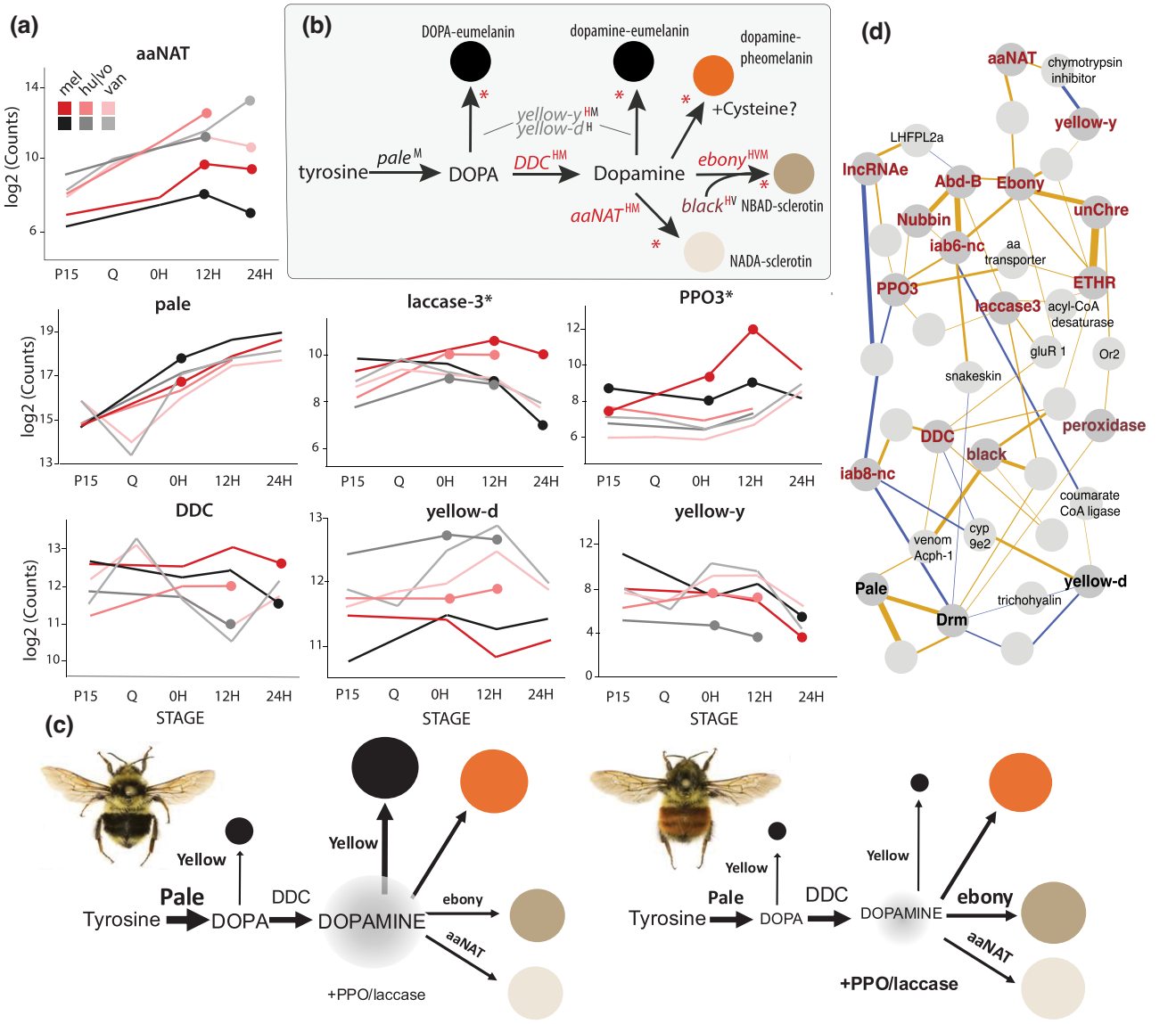

Fig. 5. Patterns of gene expression in melanin genes across mimicry pairs. a) Gene expression plots showing averages per stage and mimicry pair with dots indicating differentially expressed species/morph pairs. b) Melanin pathway showing the main enzymes, most of which are differentially expressed. Asterisks represent both *laccase* and *PPO3* points of involvement. Letters next to enzymes represent which mimicry pair is differentially expressed (H, *huntii/vosnesenskii*; M, *melanopygus*; V, *vancouverensis*) and are colored by the color form upregulated in those species. Large dots of end products show the colors of those products. c) A hypothetical schematic showing how changes in gene expression of each enzyme could lead to differences in color in the mid-abdominal segments. The size of the text of enzymes and precursors indicates their amount of expression. The size of the arrow suggests the amount of precursor being processed to the next step. The size of the dots of dopamine and final pigments indicates the hypothetical amount produced. d) Central gene network of DEGs for *B. melanopygus* and *B. vancouverensis* 0 and 12H stages, including pigment genes and core network genes (Fig. 4) and all genes directly connected to these genes but excluding nodes with one gene connection. Yellow edges are positively correlated, and blue edges are negatively correlated. The thickness of the branch reflects the summed weight of the edge across each of the analyses performed for these stages. Core focal genes are shown with dark gray circles, and the color of their names reflects whether they are upregulated in red, black, or variably. The lighter gray genes are not colored by regulation direction. Circles with no names are uncharacterized loci. The full gene network is provided in supplementary fig. S5, Supplementary Material online.

an ETHR intron. ETHR is a G-protein-coupled receptor involved in promoting ecdysis and regulating juvenile hormone. These three genes are all linked together and with the *ebony* gene in the genome (Fig. 4c). *Abd-B*, *nubbin*, *ebony*, and these ebony-linked genes are the most consistently and highly upregulated genes across all three species (Figs. 3 and 4).

Only the TF *drumstick* is consistently upregulated for black coloration across all three species. *Drumstick* is a zinc finger TF in the Odd-skipped family that regulates development and cell fate, including positional expression in response to segment polarity genes in the epidermis (Signore et al. 2012) and gut development (Öztürk-Çolak et al. 2024). It shows gene network connection (but not genetic linkage) to *pale*, one of the only pigment genes to show higher expression in black form, and a repressive interaction with the *Abd-B iab lcRNA2*.

Outside of these genes, there are several other genes found in at least two species with consistent expression patterns across species (supplementary table S3, Supplementary Material online). Most of these do not have any obvious function in relation to color, but some may play a role in color determination. *PAPSS*, upregulated in red form, is a gene involved in

sulfur processing, so it could relate to cysteine processes for red pheomelanin production. In addition, there are several genes in the melanin pathway highlighted below.

Gene Ontology Enrichment of DEGs

We performed gene ontology and gene network analysis on DEGs in *B. vancouverensis* and *B. melanopygus* for 0 + 12H for each species separately and the combined. This supports shared enriched functions between the species of embryonic pattern specification, driven by transcription factors engaging in patterning like *nubbin*, *apterous*, *drumstick*, and *Abd-B*, as well as hindgut morphogenesis. *B. melanopygus* has enrichment for dopamine biosynthetic processes, which represent the melanin pathway, long-chain fatty acid synthesis, iron transport, and sulfate-based biosynthesis (PAPSS processes), which may relate to pheomelanin production. *B. vancouverensis* has enrichment instead for succinate, retinal/carotene catabolic processes, and L-glutamate transmembrane transport. The combined dataset merges these functions. WGCNA gene network analysis recognizes three clusters, two of which provide similar GO terms and thus were analyzed together (supplementary fig. S5, Supplementary Material online). This cluster is enriched for catechol and biogenic amine (both related to the dopamine/melanin pathway), iron, and endosome transport. The dopamine pathway is known to generate oxidative stress and impact iron homeostasis and pigments, likely requiring some molecular transport into setae. The other cluster is enriched for sulfate assimilation, hindgut development, embryonic pattern specification, and intraciliary transport.

Multiple Melanin Genes Are Involved Across Mimicry Pairs

Prior work (Hines et al. 2017) found that *B. melanopygus* and *B. huntii* setae are colored primarily by pheomelanin, while the black setae of *B. melanopygus* are colored largely by eumelanin with some masked pheomelanin, and that bumble bee red and black colored setae largely utilize dopamine melanin, and not DOPA (L-3,4-dihydroxyphenylalanine) (<6%) melanin (Fig. 5b), which is less common in insects (Galván et al. 2015; Barek et al. 2018). We base our melanin pathway inferences on the established melanin pathway for insects (Futahashi et al. 2022) outlined in Fig. 5b, with some suggestive roles for pheomelanins based on vertebrate models and pheomelanin chemistry in insects (Barek et al. 2018). While these pathways are fairly well known for dark–light coloration, little data is available on genes generating pheomelanin in insects, as *Drosophila* models from which pathways are largely built make less use of pheomelanin in their coloration (Galván et al. 2015; Barek et al. 2018; Futahashi et al. 2022). In this model, pheomelanins are generated from dopamine without needing an enzyme as long as thiols like glutathione and cysteine are present (Sugumaran and Barek 2016), while dopamine is converted enzymatically into eumelanin by the *yellow* family (Futahashi et al. 2022).

Transcriptomic data reveal that many genes in the melanin pathway likely work in concert to regulate dopamine levels in the melanin pathway to lead to red and black color shifts. We hypothesize that this operates primarily by red individuals increasing the production of light melanins and lowering dopamine to prevent dark melanins. All three taxon pairs upregulate *ebony* 4 to 8 times higher in red forms, which would convert dopamine to tan-colored NBAD sclerotin. Expression of *arylalkylamine N-acetyltransferase* (*aaNAT*) is higher in red forms of *B. melanopygus* and *B. huntii*, which would further convert dopamine to clear NADA sclerotin (Fig. 5). Conversely, *pale*, which acts as a valve to allow dopamine production, is expressed at higher levels in black forms. This is only significant in *B. melanopygus* 0H, but is higher in the other two mimicry pairs in black form at this time (Fig. 5a). *Dopa decarboxylase* is elevated in red forms for some species (*B. huntii/vosnesenskii* and *B. melanopygus*), which could further reduce DOPA melanin. DOPA is known to make some eumelanin in insects, while pheomelanin is produced mostly from dopamine melanin (Barek et al. 2018); thus, reducing DOPA could reduce relative eumelanin levels. While not always significant, *yellow-d* is higher in all black forms around 0 to 24H. *Yellow-y* is significantly higher in *B. melanopygus* black form at 24H but has low expression in all *B. vosnesenskii* stages, leading to the opposite trend in *B. huntii*. Given that this is a gene family and *yellow* gene copies are known to subfunctionalize for melanization (Ferguson et al. 2011; Futahashi et al. 2022), further investigation of their roles is needed. Other DEGs from this pathway include *laccase-3* and prophenoloxidase (PPO) *3*, two gene families hypothesized to oxidize the final steps of melanin production across melanin and sclerotin end products, and which are higher in red form. *Peroxidase* is likely involved in enabling oxidative processes and plays variable roles across species by color, as does *cysteine sulfinic acid decarboxylase*, orthologous to the gene *black*, which is thought to work with *ebony* to make light tan cuticle.

The Hox Locus Utilizes ncRNA Differential Expression

In addition to *Abd-B*, we uncovered two differentially expressed lncRNAs that span the regulatory region between *abd-A* and *Abd-B*. These were identified by merging all reads from across each taxon and using read break points and paired ends to manually annotate the ncRNAs. Merging was necessary as the transcript abundance is very low, as is typical for lncRNAs (Jarroux et al. 2017). ncRNAs were validated using custom PCR of cDNA from the transcriptomes and bumble bee genome annotations of these species. PCR amplicons matched closely to bioinformatic annotations (supplementary fig. S7, Supplementary Material online). *Bombus impatiens* lacked these ncRNAs in the genome annotation, but other species have these partly defined (supplementary fig. S7, Supplementary Material online).

In *Drosophila*, an lncRNA (*iab8-ncRNA*) is transcribed and spliced across this region. Each exon occurs in a regulatory region that directs expression in a different body segment for each of these genes (Fig. 6) and the order of the regulation matches the order of the segments along the body, thus these regulatory domains act in a colinear fashion in the same way as the Hox gene proteins (Garaulet and Lai 2015). One of the bumble bee ncRNAs likely functions similar to *Drosophila iab8-ncRNA* in that it appears to transcribe across this ~250 kb region and splice at exons dispersed across the full interval (Fig. 6). This transcript includes initial exons in the UTR region of *abd-A* and an alternative start site in the coding region of an uncharacterized protein between Hox genes *abd-A* and *Ultrabithorax* (*Ubx*), and terminates close to the start site for *Abd-B* (20 kb). Most of the intergenic (iab) exons of this *iab8-ncRNA* are consistently spliced across species and color forms; however, we found an alternative transcript that terminates 1.2 kb prior to the identified deletion region and within the *B. melanopygus* 5 kb region of fixed association (Fig. 6). This splice variant is found in most forms

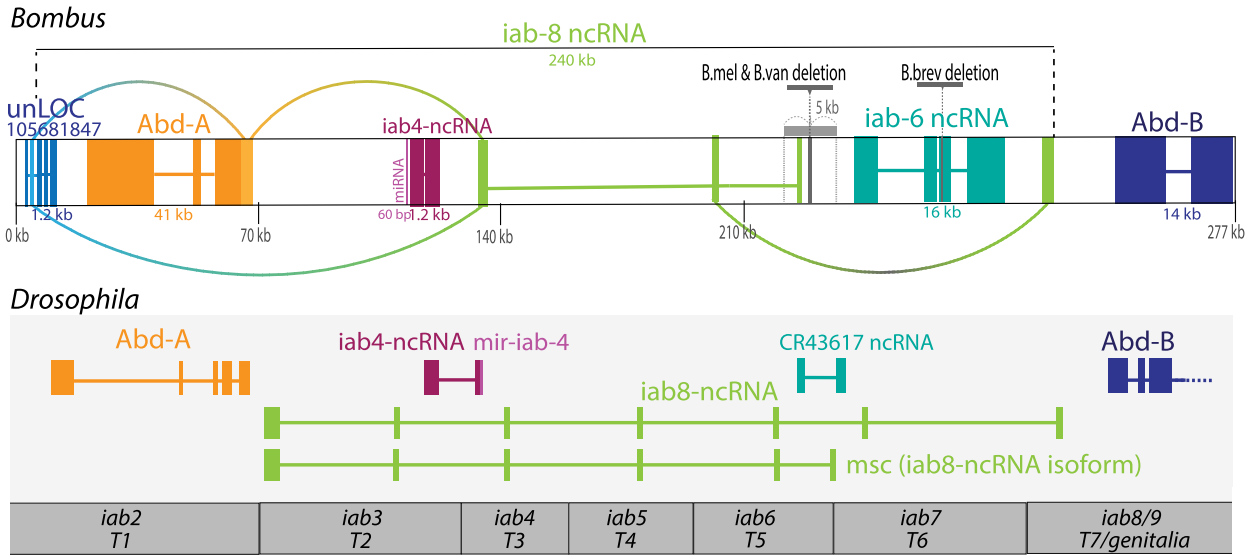

Fig. 6. Schematic of ncRNAs in the bithorax complex of bumble bees compared alongside the iab transcripts in *Drosophila*. The position of the deletions driving red–black variation in *B. melanopygus*, *B. vancouverensis*, and *B. breviceps* and the positions, exons, and splice variants of the lncRNAs are shown. At the bottom is the *Drosophila* infra-abdominal (iab) region with potential orthologs colored similarly. Beneath it is the segmental iab domain from *Drosophila*, each of which regulates expression of these genes in a different numbered abdominal segment. Beneath that is the inferred respective bumble bee segment it corresponds to. Bumble bee *iab8-ncRNA* shows similar patterns of expression to *iab8-ncRNA* in *Drosophila*, which also has a shortened male-specific abdominal (*msc*) isoform (Graveley et al. 2011), although this does not mean they are orthologous. *Drosophila* has an ncRNA (*iab-4*) that flanks the miRNA (*mir-iab-4*) in this region, similar to the flanking ncRNA in *Bombus*. This miRNA was confirmed bioinformatically to be homologous, as were *abd-A* and *Abd-B*. The other ncRNAs were too dissimilar to align using sequence-based alignment, and thus are inferred to be similar (but not necessarily orthologous) based on properties and position. Data for the figure is derived from Garaulet and Lai (2015), Graveley et al. (2011), and annotations from the *D. melanogaster* genome r6.62.

and species but both splice variants are differentially expressed, with patterns matching *Abd-B* expression. For these variants, all three mimicry pairs have 2 to 3× higher expression in red than black forms.

A second ncRNA, *iab6-ncRNA*, is nested within the transcriptional range of *iab8-ncRNA*, between the color interval and the final exon. This lncRNA includes the color locus found to drive red–black tail variation in another bumble bee species, *B. breviceps*, and was differentially expressed in that study (Yang et al. 2023; Fig. 6). If this regulatory region works as in *Drosophila*, this would be implicated primarily in transcribing the regulatory region for *Abd-B* and metasomal segments 5 and 6. *Drosophila* has an ncRNA in this region as well with unknown function (CR43617). We found similar splicing across species and color forms (supplementary fig. S6, Supplementary Material online), but higher expression of this transcript in red forms of all three species. The strength of co-expression between *iab6-ncRNA* and *Abd-B* is the second strongest in this gene network, second to *ETHR* and its neighboring uncharacterized protein. A third *ncRNA* adjacent to the evolutionarily conserved miRNA in this intergenic region was not differentially expressed.

Evolution of Gene Networks

When examining the expression of genes in the core pathway in a phylogenetic perspective (Fig. 7), we find these genes to be upregulated independently in the three red form species from a background of lower signal. In the melanin genes, there are some phylogenetic trends but also differences in deployment in each of these by species. For example, PPO3 is higher in the *B. melanopygus–B. bimacultatus* lineage and more importantly for phenotypic differences in *B. melanopygus*. *aaNAT* is higher in the alternate lineage but is upregulated independently in *B. melanopygus* and *B. huntii* red forms. *Pale* appears to be downregulated in each of the red form lineages, whereas *drumstick* appears to be upregulated in black forms of polymorphic clades. This mapping also supports more effects on gene expression in *B. melanopygus* and *B. huntii–vosnesenskii* than can be found in *B. vancouverensis*.

Discussion

By utilizing this replicate-rich mimicry system, we have uncovered trends in how genomes are targeted to create adaptive variation. We show that the Hox regulatory locus of *Abd-A-B* is a hotspot of evolution, repeatedly and independently targeted to drive red to black abdominal color variation in these bees. Deletions in the same locus for two mimetic species correspond to differences in *Abd-B* gene expression, and a third mimicking species pair shows marked differential expression that also suggests involvement of this gene. How this locus operates is yet to be determined, but the discovery of two differentially transcribed ncRNAs across this 250 kb interval and near the color locus suggests that ncRNA regulation may be involved. TF binding analysis suggests that homeobox gene binding may regulate these transcriptional differences. Analysis of red–black polymorphisms in *B. breviceps* also involved this intergenic region and an ncRNA (*iab6-ncRNA*) (Yang et al. 2023). As *B. breviceps* is a fairly distant lineage from those studied here (~22 my divergent, Hines 2008a), this suggests that this genetic region is likely implicated in segmental color phenotypes more broadly across the *Bombus* lineage.

Bombus breviceps color variation occurs in the last 2 to 3 abdominal segments (M4 to 6), while for species studied here red–black variation occurs in the mid-abdomen/metasoma (M2 + M3). Involvement of *Abd-B* for *B. breviceps* is not unusual, given that this is a tail phenotype and terminal segments are the typical zone of *Abd-B* expression. The more anterior

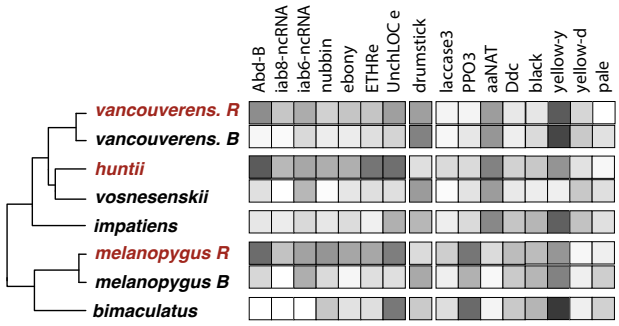

Fig. 7. Evolution of gene expression patterns during early callow stages across core and pigment genes. The heat map indicates the level of 0 + 12H averaged expression across core gene sets and melanin genes, scaled as fold change from the lowest expression for each gene. Most genes are similar across these stages, except *pale*, thus *pale* is for 0H only. *B. bimaculatus* was only sampled at 0H. Breaks separate the core genes upregulated in red form, *drumstick*, which is the main shared TF upregulated in black form, and the remaining melanin genes.

Abd-B upregulation in *B. melanopygus*, *B. vancouverensis*, and *B. huntii* here is atypical. For *Drosophila*, this regulatory region is colinear, where the parts closest to *Abd-B* regulate expression of this gene in the most posterior segments, and the parts between *Abd-A* and *Abd-B* are most likely to regulate more anterior expression of *Abd-B*. The location of the different variants here (anterior red stripe regulated more internally than the posterior red color; Fig. 6) matches this regulatory framework.

Nevertheless, the involvement of *Abd-B* suggests that the spatial expression of Hox genes is altered from their typical domains of expression, which normally generates a homeotic transformation. However, because *Bombus* color determination occurs at the end of development, shifts in the expression location of this gene should only impact this phenotype. Major selector genes may have greater flexibility in how they are utilized later in development (Werner et al. 2010). Involvement of a major developmental segmentation gene is a good strategy when pleiotropy can be avoided, as these genes likely have evolved connections with downstream phenotypic genes (Tian et al. 2019). In this case (Fig. 8), *Abd-B* may have evolved a binding site in *ebony* that led to its upregulation to make a red tail. A red tail, a potential warning signal of the sting, is the most common location for red color across bumble bees and is thought to represent the ancestral bumble bee phenotype (Williams 2007). Subsequently, red color may have evolved in the mid-abdomen through mutations that shift *Abd-B*, and subsequent *ebony* expression, anteriorly. This aligns with what has been observed in *Drosophila* wings, where the major regulatory wingless evolved first to define wing locations and build wing phenotypes like cross-veins, was co-opted to turn on melanin in some of those veins, and subsequently, this regulatory changed the location of its expression to create melanic wing patterns (Werner et al. 2010; Arnoult et al. 2013). As Hox genes drive segmental fates, moving Hox genes along the body axis late in development is a potential means to adjust segmental colors to create new patterns. In the case of mimicry, changing the same loci that lead to mobile expression of Hox genes repeatedly enables multiple species to converge on this new pattern under the selective forces of frequency-dependent selection.

Abb-B has been found to have regulatory interactions with realizator genes, including *bab*, sex determination gene *dsx*, and a POU domain gene *pdm3* to drive abdominal pigmentation pattern variation by species and caste in *Drosophila* (Kopp et al. 2000; Liu et al. 2019), but it has also been found to directly bind in *-cis* to direct the expression of downstream melanin genes such as *yellow* (Jeong et al. 2006; Rogers et al. 2014; Liu et al. 2019). Expression domains of *Abd-B* have been found to vary in pupal stages in *Drosophila santomea*, leading to the suggestion that upstream gene expression shifts, such as those we observe with bumble bees, combined with downstream shifts in binding of *Abd-B* to pigment genes, contribute to the evolution of color pattern phenotypes in *Drosophila* (Liu et al. 2019).

Using transcriptomics of convergent phenotypes can reinforce how gene targets translate to shifts in transcription to impart these phenotypes. We revealed the genes central to the gene network, not only because they are highly differentially expressed, but because they are differentially expressed each time the phenotype arises. In this case, *Abd-B* leads to changes in *ebony* and *nubbin* for all three mimicry pairs, supporting a potentially conserved ancestral network that engages a realizator and downstream pigment gene, similar to *Drosophila*. Nevertheless, *ebony* is not the only pigment gene involved in red coloration. Targeting an upstream developmental gene can drive widespread effects on gene expression. In *Drosophila*, often it is the pigment enzyme, either *yellow*, *tan*, or *ebony*, targeted in *cis-*, that is involved in driving melanic color variation (Kronforst et al. 2012; Massey and Wittkopp 2016). In such cases, the effect is likely to be localized to that enzyme, whereas targeting upstream developmental genes has the potential to elicit broader effects.

We find that most genes in the melanin pathway are differentially expressed, but not all are implicated across all three mimicry pairs. Potentially, these genes are recruited to reinforce and stabilize this phenotype. Alternatively, these could be co-regulated by shifts in the expression of metabolites or other enzymes in the pathway. The variation across species presents a means by which novel regulatory pathways can evolve. There are several cases where homologous phenotypes are underlain by considerably different molecular pathways (e.g. developmental systems drift; True and Haag 2001). Having the same homologous structure, with little similarity in genes that make it, can happen through multiple alleles (and variance in these across populations) that function in combination or with redundancy to generate an effect. For example, genes with redundant or reinforcing function can assist in the phenotype, can shift to becoming the primary functional genes, and the original gene driving the function can be lost. The alternate means to lower dopamine to favor light over dark color, seen here, shows how such shifts might take place over time.

Our research highlights *ebony* as being an important gene for promoting red color variation in these bees and insects in general. *Ebony* upregulation leads to lighter tan phenotypes in *Drosophila* (Kronforst et al. 2012; Massey and Wittkopp 2016) but not in red color. Recent studies with CRISPR or protein mutations in *ebony* reveal the extensive roles this gene plays in dark/light phenotype variation across the insect body, life-history stages, and species (e.g. tephritid fly, Paulo et al. 2025; *Plutella* moths, Xu et al. 2021; lady beetle, Lin et al. 2025; silkmoth, Osanai-Futahashi et al. 2012) and *ebony* is involved in light coloration in natural variants of multiple Lepidoptera (Futahashi and Osanai-Futahashi 2021; Futahashi et al. 2022) and honey bees (Rosa et al. 2021). It was previously found to drive red coloration in *Papilio* caterpillar eyespots (Futahashi and Fujiwara 2005). Pheomelanin production should also require a source of cysteine. There were no

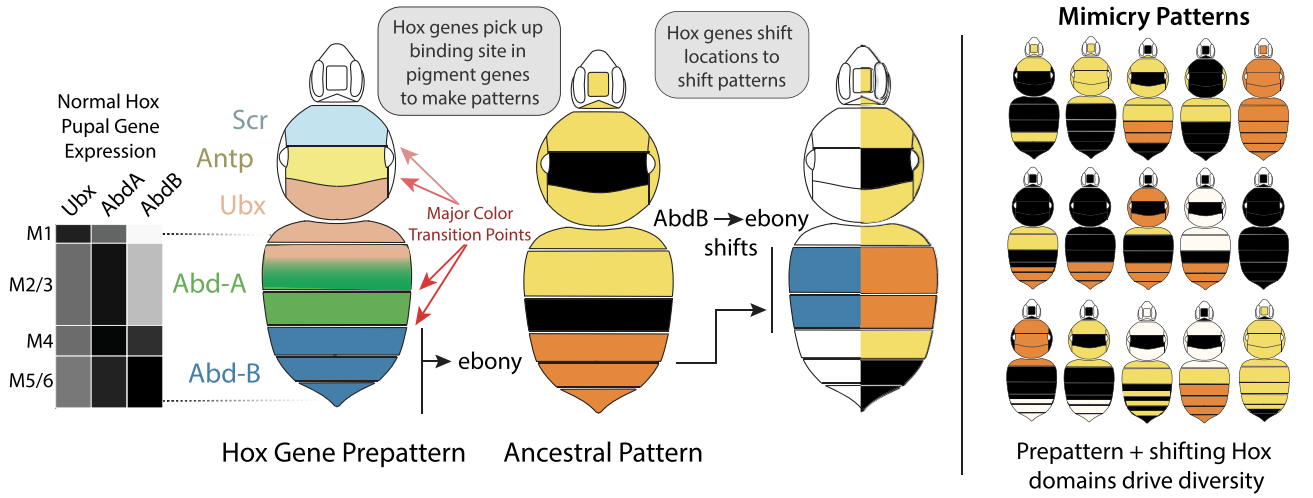

Fig. 8. Schematic of how color pattern diversity is generated in bumble bees. Segmental coloration in bumble bees is most likely generated using Hox genes that turn on pigment genes. *Abd-B* likely evolved to trigger *ebony*, making red in the tail where *Abd-B* is expressed. Subsequently, shifts in the location of *Abd-B* moved the red color to new locations. *Far left*—The gene expression pattern of the bithorax genes across the metasoma/abdomen of a bumble bee inferred from Tian et al. (2019). Note that Tergite (T) 2 and 3 were merged in this analysis, as were T5 and 6. *Left*—The inferred Hox gene domains for bumble bees. *abd-A*/*Ubx* boundaries in T2 are unclear with the current data, but a gradient is likely considering the color patterns found in bumble bees. In red, the major points of color transition across all bumble bee color patterns, inferred by Rapti et al. (2014), are indicated. *Middle*—The most common bumble bee pattern, which is also likely to be the ancestral color pattern (Williams 2007). *Right*—A schematic of how shifting *Abd-B* from its typical location leads to the Rocky Mountain color pattern. *Far Right*—15 of the 24 major mimicry patterns in bumble bees globally.

obvious candidates that worked with the core pathway to promote this, although *PAPSS* and *glutathione-S-transferases* may operate in this role.

The involvement of *nubbin* in coloration has not been found outside of these bees. This gene is most noted for its role in wing development (Ng et al. 1995), but as a major homeodomain TF known to drive cell fate, it plays roles in other phenotypes. The TF *apterous* is also upregulated in red form, and it too is known to regulate wing phenotypes (Klein et al. 1998). In *Drosophila*, another POU domain homeobox protein, pdm3, has been found to drive genetic variants in abdominal pigmentation (Yassin et al. 2016), suppress *yellow* and eumelanin expression (Rogers et al. 2014; Liu et al. 2019), and to potentially be regulated by *Abd-B* (Yassin et al. 2016). Further research is needed to understand the evolutionary gain and role of *nubbin* in abdominal pigmentation networks.

Three genes linked to *ebony* showed similar gene expression patterns to *ebony*: ecdysis-triggering hormone receptor *ETHR*, an *lncRNA* in ETHR, and an uncharacterized locus that in honey bees is called *Thelytoky* (Aumer et al. 2019). ETHR is involved in regulating juvenile hormone and ecdysis and thus may be implicated in caste determination, reproduction, and sociality. *Thelytoky* was found to drive the regain of worker reproduction in honey bees in a honey bee colony (although see Yagound et al. (2020) and Christmas et al. (2019) for alternative explanations), and the close association with *ebony* explains how these same workers exhibit shifts in melanin phenotypes (Rosa et al. 2021). It is possible these genes show co-expression with *ebony* solely through linkage. If this were the case, increasing *ETHR* with *ebony* expression could change aspects of reproduction and response to ecdysis, and thus have pleiotropic effects related to behavior. Changes in *ETHR* could also change tissue responsiveness to the ecdysis-triggering hormone, thus play a functional role in regulating the timing of color expression.

The intergenic region between *Abd-B* and *abd-A* has previously been studied in *Drosophila* (Garaulet and Lai 2015). While Hox gene evolution has been studied across arthropods, little is known about similarities in how this intergenic region operates. At a sequence level, there is little similarity of bumble bees to *Drosophila*, with alignments only possible in Hox transcripts and in the miRNA in this region (Fig. 6); thus, it is not possible to establish homology across this region. However, the presence of a similar lncRNA in bumble bees to *Drosophila iab-8 lncRNA*, spanning a similar unusually large range of bases (250 kb primary RNA transcript), suggests that the mechanism of regulation may be conserved. These data add to an increasing number of studies implicating ncRNA regulation in driving phenotypic variation (Luo et al. 2019; Du et al. 2023; Li et al. 2023; Monniaux 2023).

In this study, the mimics present different challenges for evolutionary genetic inferences given their phenotypic variation and gene flow. For GWAS, we assessed the easy case of dimorphic individuals from a region of admixture at a point of secondary contact (*B. melanopygus*; Ezray et al. 2019), compared with a continuous phenotype over a larger range with geographic structure (*B. vancouverensis*). For GWAS, *B. vancouverensis* compared with *B. melanopygus* showed much less LD (supplementary fig. S2, Supplementary Material online), leading to only a single variant, rather than the broad peak found in *B. melanopygus*. In *B. vancouverensis*, other, likely lower frequency, variants must be involved, given a lack of fixation of the one indel. Finding these additional loci will require examining individuals with color differences that lack the implicated deletion and may require more local regional assessments to tease out the effects of multiple loci that vary across the geographic range. Incorporating transcriptomic sampling across key pigment-developmental stages provides a valuable complement to sequence-based analyses. Although key members of the core network were similarly differentially expressed in *B. vancouverensis* and *B. melanopygus*, *B. vancouverensis* again proved more complicated with fewer DEGs. The lack of completely dimorphic phenotypes sampled may have produced this dampened response. Further, *B. vancoverensis* is a highly heterozygous, large effective population size species (Lozier et al. 2011,

2023) that has a broad geographic range, and it is possible that different populations have dissimilar gene expression strategies. For transcriptomics, we also assessed red–black sister species *B. huntii* and *B. vosnesenskii*, showing that species transcriptomics yields a lot of species-specific gene expression patterns likely unrelated to the color phenotype, but that comparing gene expression across species can still be valuable.

Understanding the role of the implicated genes would best be confirmed with functional genetic approaches, such as RNAi and CRISPR-Cas9. These techniques, however, can be challenging in these bees, as they are difficult to rear in large numbers and cannot easily be propagated across generations. In our experience, RNAi injections during nonfeeding pupal stages induce a melanin-based immune response that causes color changes even in control treatments, and CRISPR is limited by the need for progressive larval care and ejection of disturbed eggs by workers. While functional genetic techniques will be important for future research on these bees, our study shows the value of a comparative approach to yield considerable insights with more approachable techniques in nonmodel organisms.

Overall, this study implicated Hox genes in color pattern variation in bumble bees. In the future, this system can be used to understand the mechanisms of abdominal Hox gene regulation and their role in generating phenotypic variation. This study finds a core network in these bumble bees, which is in need of study for its broader involvement across this mimetic radiation. This replicate-rich system shows how gene targets and their networks can evolve to impart adaptive phenotypic diversity.

Methods

Genomic Analysis

Heredity Analysis in B. vancouverensis

To assess heredity, we collected individuals reared from 34 colonies and scored their percent red and black coloration by sex and caste. For each colony with variable coloration across individuals, we calculated the proportion of bees by color bins (0, <10, 11 to 25, 26 to 50, 51 to 75, 76 to 90, and 91% to 100% red) as well as an overall colony mean by caste and sex and compiled these data for visualization. Wild collected male and worker bees from across this color-variable range were assessed for color phenotype by the geographic region to determine sex effects on color.

Genomic Analysis for Identifying the Color Locus in B. vancouverensis

Sampled black forms ($n = 24$) were 0% red (percent red = area of segment red/(red + black)) in the second and third metasomal segments. Red forms ($n = 24$) were ≥88% red in these segments for 23 individuals, with one individual being 70% red in the transition zone. DNA extractions of these individuals were performed on bee legs and/or muscles using Omega Biotek EZNA DNA extraction or Qiagen DNeasy kits with standard protocols, with RNase removal. All genomes were sequenced with 150 bp paired-end Illumina sequencing at mean ~17 times coverage (ranging from 11.7 to 44.9×). We ran four separate multiplexed sequencing runs from 2018 to 2022, with DNA libraries prepared using Truseq, Nextera, or Illumina DNA kits and sequencing conducted using the HiSeq 2500, NextSeq 550, or NextSeq 2000 P3 sequencer, respectively, at the Penn State Huck Genomics Core Facility (University Park, PA) (supplementary table S1, Supplementary Material online).

Initial quality assessment and preliminary statistics of the raw sequencing reads were obtained using FastQC v.0.11.9 (Andrews, 2010) and SeqKit v.0.15.0 (Shen et al. 2016). Paired-end read libraries from all samples ($n = 48$) (supplementary table S1, Supplementary Material online) were trimmed using Trim Galore v.0.6.6 (Krueger et al. 2021) to remove low-quality bases (Quality Phred score cutoff = 20) and Illumina library adaptors, and reads were discarded that did not pass a minimum length of 20 bp. Filtered reads were aligned to the *B. vancouverensis* genome assembly (RefSeq GCF_011952275.1, Heraghty et al. 2020) using the BWA aligner v 0.7.17 (Li and Durbin 2009) on bwa-mem setting (Li 2013) with parameters (-t 8 -K 100000000). Various postprocessing steps of alignment files (e.g. sorting and indexing, marking duplicates) were conducted using Picard tools v.2.23.9 (available from: broadinstitute.github.io/picard/index.html).

Variant calling from these sample-specific alignment files were conducted using GATK v.4.4.0.0 (McKenna et al. 2010) using the HaplotypeCaller option with haploidy-specific settings (–ploidy 1) to generate per-sample Genomic VCFs (GVCFs). These GVCFs were aggregated using GenomicsDBImport functionality, and the GenotypeGVCFs option was used for joint genotyping across all samples to produce a unified cohort-wide variant calling dataset. This raw variant call file was filtered using VCFtools v. 0.1.16 (Danecek et al. 2011) using parameters (–max-non-ref-af 0.95 –minDP 2 –minGQ 20 –minQ 30 –max-missing 0.75) to yield 4,753,164 SNPs and 638,680 indels. This filtered dataset was run through a genotype–phenotype association analysis using case versus control phenotypes (i.e. black and red) and a Fisher's exact test in PLINK v1.90b6.21 (Purcell et al. 2007), using the –adjust command to generate Benjamini-Hochberg adjusted *P*-values for false discovery rate correction (Benjamini and Hochberg 1995). The FASTMAN R package v. 0.1.0 (Paria et al. 2022) was used to generate the Manhattan plot. To visualize geographic structure in these genome samples, a principal component analysis was conducted in PLINK by filtering the raw variant call file for population structure analyses, including a minimum depth of 4 (–minDP 4), no missing data (–max-missing 1.0), minor allele frequency of 5% (–maf 0.05), and no more than one SNP per 5 kb to reduce linkage effects (–thin 5000).

We used manual inspection of read alignments in Integrated Genome Viewer (Robinson et al. 2011) from our genome sequences within 25 kb of the most associated variant to determine there was no evidence of missed color-associated large deletions (inferred from read loss), large insertions or transposable elements (inferred from unmatched read pairs and regions of read termination or misalignment), or uncalled variants near the associated site.

To visualize genotype patterns within the *Abd-B* regulatory region using the genomic data, we used the *Genotype Plot v0.2.1* (Whiting 2022) after converting alignments of the color locus (20 and 4 kb surrounding the deletion) into a biallelic VCF using *snp-sites v2.5.1* (Page et al. 2016) and *bcftools v1.16* (Danecek et al. 2021). LD within these genetic regions was assessed for *B. vancouverensis* and compared with previously published *B. melanopygus* data (Tian et al. 2019) by computing pairwise r^2 values using PLINK v1.9 and plotting their patterns in *ggplot2*.

Transcription Factor Binding Analysis

We conducted TFBS prediction on representative sequences of both color forms (black form BIF_B8_11, 127 bp; red form HH16_16_2, 134 bp). First, insect-specific TF motifs (n = 286) from the JASPAR CORE collection (Rauluseviciute et al. 2024) were obtained and converted to position weight matrices with *Bombus* optimized parameters (Crowley et al. 2023), including nucleotide frequencies A = 0.31, C = 0.19, G = 0.19, and T = 0.31. Representative sequences were scanned for TF binding sites using the searchSeq functionality of TFBSTools v1.40.0 (Tan and Lenhard 2016), with a minimum score threshold of 0.9. Predicted TFBS were exported in GFF3 format to be aligned and visualized (Fig. 2e), and total TFBS counts per site and their identity were inferred manually in Geneious (available from: https://www.geneious.com).

Additional Sequence Comparison in Color Locus and for lncRNA

To improve understanding of the inheritance and evolution of the identified indel region in *B. melanopygus* and *B. vancouverensis*, we PCR amplified the region with primers that spanned a 1,440 bp fragment, including these indels (Tian et al. 2019): 1to2_2 5′-CCGTAGCTGTTACCGAACAA-3′, 5′-GGGCTGACTTTCAACCAAAT-3′ (50 to 52C amplification temperature). These were run on nine samples run for genomic sequencing, including samples that deviated from fixation, to confirm the bioinformatically inferred indels. We sampled 16 new individuals: 8 red (7 males, 1 female), 5 black (2 males, 3 females), and 3 intermediate males *B. vancouverensis* (supplementary table S3, Supplementary Material onlineb). To infer the evolution of the color locus across the clade, we sampled eight additional species and their respective color variants (see Fig. 2d; supplementary table S3, Supplementary Material onlineb). These amplifications were purified with Exosap-IT (Thermo-Scientific) using recommended protocols and sequenced using Sanger sequencing procedures at the PSU Huck Genomics Sequencing Center (University Park, PA). Sequences were edited and aligned to the interval in Geneious to infer indels, with polymorphisms called using chromatogram double peaks.

In addition, we examined sequence variation in ~200 bp spanning the indel using published whole-genome assemblies from NCBI database (Christmas et al. 2019 for *B. sylvicola*; Koch et al. 2024 for *B. huntii*, Heraghty et al. 2020 for *B. vosnesenskii*, *B. bifarius*, and *B. vancouverensis*; Toth et al. 2024 for *B. impatiens*) or Illumina paired-end sequencing data obtained from NCBI SRA (Tian et al. 2019; Ghisbain et al. 2020; Heraghty et al. 2020, 2023) and newly sequenced whole-genome shotgun sequencing data. In total, using reference assemblies and resequenced individuals, we examined members of the *Pyrobombus* clade, including comparing four *B. vancouverensis* black, three *B. vancouverensis* red, three each of *B. melanopygus* red and black, four *B. huntii*, four *B. vosnesenskii*, four *B. impatiens*, four *B. bifarius*, three *B. ternarius*, three *B. bimaculatus,* and one red *B. sylvicola* (supplementary table S3, Supplementary Material onlinea). Newly sequenced libraries were prepared using the NEBnext Ultra II FS DNA kit with unique dual index oligos (New England Biosciences) from whole-genomic DNA isolated from thoracic muscle and legs using the Qiagen DNeasy Animal Tissues protocol. Paired-end 150 bp sequencing was performed on an Illumina NovaSeq X by Psomagen, Inc. (Beltsville, MD).

After trimming and quality control of reads using the default Trim Galore! v.0.6.6 (Krueger 2015) options, we mapped reads for each sample to the phylogenetically closest reference genome for each species (supplementary table S3, Supplementary Material online) using BWA-MEM (Li 2013), followed by MarkDuplicates and BuildBamIndex commands in Picard Tools v. 2.23.9 (Broad Institute 2020). We then used the SAMtools v.1.21 (Li et al. 2009) command consensus -f fasta to extract fasta formatted consensus files (with gaps and IUPAC base and ambiguity codes) for the target region (specifying the focal region around *abd-A* and *Abd-B* for each reference genome for each species) using the default Bayesian consensus caller that includes the use of base quality adjustments and mapping qualities. The sequences were combined into a single multi-sequence fasta file and aligned using MAFFT v7.525 (Katoh and Standley 2013).

To refine the exon composition, splicing location, and potential splice variation of the three identified iab lncRNAs, we designed multi primer sets spanning the bioinformatically inferred genomic ranges and PCR amplified and sequenced each of these regions across two samples per morph for *B. melanopygus* and *B. vancouverensis*, two *B. huntii*, and two *B. vosnesenskii*. See supplementary fig. S7, Supplementary Material online for primer locations, sequences, and results.

Transcriptomic Analysis

Sample Preparation and RNA Sequencing

Queens of each species and color form were collected from the field from source populations in Oregon, Utah, and Pennsylvania, and were reared in the lab under controlled conditions (65% humidity, 28 °C, dark). We sampled males from 2+ source colonies per species/morph, seeking to balance colony representation across stages (supplementary table S6, Supplementary Material online). Male pupal clusters from these colonies or from worker mini-colonies assembled from these source colonies were isolated during mid-pupal stages in an incubator with the same conditions. They were determined as to when they reached pupal P15 or quiescent staging through a small hole in cocoons, or by monitoring removed pupae close to this stage, placed in a humidified ceramic tray, following the staging protocol described in Tian and Hines (2018). Clusters were checked every few hours when near eclosion, and when they had fully chewed and pushed their way out of the cocoon, they were either sampled for the 0H stage or isolated with a 50% sugar solution until they reached 12 or 24H. Staging was accurate within 1 h for 0H and within 2 h for 12 and 24H. For dissection, we isolated the epidermal layer by removing these cuticular segments in chilled 1× phosphate-buffered saline and cleaning off all muscles, trachea, and other tissue; we thus sampled epidermis plus attached setae and cuticle. These fresh tissues were flash frozen on dry ice and stored at −80 °C.

RNA was extracted using the Zymo Direct-zol Microprep R2060 Kit with DNase removal steps, eluted in 15 µl of water. After quality assurance using the Agilent Tapestation, libraries were prepared using an Illumina Stranded mRNA library kit, and sequenced at The Huck Institutes Genomics Core Facility using either the NextSeq 2000 or Nextseq P4 XLEAP sequencers paired-end with 100 bp reads to a final mean of 20× genomic coverage (range 12 to 28×), and ~20 million reads per sample (range 11.5 to 50 million reads; supplementary table S6, Supplementary Material online).

Quality Control and Read Processing

Raw sequencing data quality was assessed with FastQC v.0.11.9 (Andrews 2010) and MultiQC v.1.21 (Ewels et al. 2016). Low-quality bases and adaptors were removed using Fastp v.0.23.2 (Chen et al. 2018) with the following parameters: *–qualified_quality_phred 25 –length_required 36 –trim_front1 3 –trim_tail1 3 –trim_front2 3 –trim_tail2 3 –trim_poly_g –cut_tail –cut_tail_mean_quality 20 –cut_tail_window_size 4*. Post-trimming quality was evaluated using the same QC tools.

Alignment and Differential Gene Expression Analysis

Trimmed reads were aligned using HISAT2 v.2.2.1 (Kim et al. 2015). To perform alignments, we used the *B. impatiens* (RefSeq accession: GCF_000188095.3) genome for all species. This species is contained within this *Pyrobombus* radiation (~10 my crown node of analyzed taxa; Hines 2008a). We also ran alignments of *B. vancouverensis* samples to its own (black form) genome (RefSeq accession: GCF_011952275.1) and *B. vosnesenskii* and *B. huntii* to the *B. huntii* genome (RefSeq accession: GCF_024542735.1). We tested the effects of aligning *B. vosnesenskii* (RefSeq accession: GCF_011952255.1) and *B. huntii* (RefSeq accession: GCF_024542735.1) to their own and each other's genomes. Gene sets were fairly similar, but due to differing isoforms and annotations by genome, it was not as reliable to compare expression when each is aligned to their own genomes.

Count matrices were generated using *featureCounts* v2.0.1 (Liao et al. 2014). The full dataset across all samples, aligned to the *B. impatiens* genome, was normalized together using median ratio normalization in DESeq2 v1.38.3 (Love et al. 2014) R package. This file was used for cross-sample comparison of counts and expression patterns. Only genes with at least 3 of 14 samples having a count of 30 or more reads were retained for differential gene expression analysis to avoid over-inflation of inference from unreliably low counts.

Gene expression analyses were performed in *DESeq2* for each stage, species/morph pair, and reference alignment set separately, with embedded DEseq additional normalization performed during each analysis. We also ran a separate analysis with samples from 0 and 12H run together. DEGs that passed the thresholds $P\text{-adj} < 0.05$ and $\text{abs}(\log_2 FC) > 1$ were retained. All genes differentially expressed when aligned with either alternative genome were included in DEG lists. Approximately 22% of genes were unique to one dataset: 109/488 for P15 and 207/935 for 0 to 12H in *vosnesenskii–huntii*; 3/6 P15 and 6/41 0 to 12H in *vancouverensis*. To resolve annotation inconsistencies across different references, unassociated genes between the two reference sets were blasted against each other, *B. impatiens*, and *Drosophila melanogaster* nucleotides to identify any missed orthologous gene pairs, using *B. impatiens* gene identifiers when possible.

PCA, Hierarchical Clustering, and Volcano Plots

Cross-sample normalized matrices were formatted for analysis in *readr* v2.1.4 (Wickham et al. 2024b) and *dplyr* v1.1.4 (Wickham et al. 2023) R packages. PCA was performed using the *FactoMineR* v2.8 package (Lê et al. 2008) and visualized with *ggplot2* v3.5.2 (Wickham 2016) and *factoextra* v1.0.7 (Kassambara and Mundt 2020). Hierarchical clustering dendrograms were generated using *ggplot2*. Volcano plots were generated for P15 as well as for 0 and 12H data overlaid, with a plot for each mimicry pair separately, assembled using the *EnhancedVolcano* v1.16 package (Blighe et al. 2018). In these plots, lines distinguish genes with absolute log-fold change >1 and an adjusted *P*-value of 0.05. The visualization and export of these plots were achieved by using *gridExtra* v2.3 (Auguie and Antonov 2017), *svglite* v2.1.3 (Wickham et al. 2024a), and *ggplot2* v3.5.2.

Gene Ontology Analysis

To interpret the biological significance of our gene expression data, we performed GO enrichment analyses on all significant DEG sets for 0 and/or 12H datasets for *B. melanopygus*, *B. vancouverensis*, and both species combined, using a consistent background set ($n = 9{,}803$) comprising all expressed genes with GO annotations via the *GOfuncR* v1.18 R package (Grote 2024). GO terms for the genes were obtained from the *B. impatiens* RefSeq assembly available at the NCBI FTP site (https://ftp.ncbi.nlm.nih.gov/genomes/all/GCF/000/188/095/GCF_000188095.3_BIMP_2.2/GCF_000188095.3_BIMP_2.2_gene_ontology.gaf.gz). The custom background GO annotation file was processed using the *dplyr* v1.1.4 R package, filtering for GO terms with raw $P\text{-values} < 0.05$.

To examine functional enrichment of different gene network clusters, we constructed co-expression networks using *WGCNA* v.1.72.5 R package (Langfelder and Horvath 2008) on normalized expression matrices for the combined *B. vancouverensis* and *B. melanopygus* 0 and/or 12H DEG set. Soft-thresholding was determined via scale-free topology analysis, and modules were identified using the *blockwiseModules* function, and enrichment was performed as outlined above.

Enriched GO terms were visualized using the GO-Figure! tool (Gabriel et al. 2021). We selected the threshold of 0.2 for the term clustering, which was the best level to enable unique functional clustering terms, but used 0.05 for the second cluster from WGCNA (supplementary fig. S6, Supplementary Material online).

Gene Network Analysis

Gene network analysis was performed on all DEGs in 0 and/or 12H stages for *B. melanopygus* and/or *B. vancouverensis*. DEGs from *B. huntii–vosnesenskii* (red vs. black form) comparisons were not compiled into this list due to likely abundance of phenotype-unrelated DEGs. Networks were constructed for *B. vancouverensis* and *B. melanopygus* separately at 0–, 12–, and 0 + 12–h, and for the combination of 0 + 12-h for both species. Co-expression networks were constructed by computing covariance matrices using the Spearman correlation method, a nonparametric approach well-suited for gene expression data that may not follow a normal distribution. Networks were constructed by applying the EBICglasso algorithm (Friedman et al. 2011) to estimate a sparse inverse covariance (precision) matrix using the *qgraph* v1.9.8 R package (Epskamp et al. 2012).

For visualization, we performed several filters to show how key genes of interest were correlated. We retained only gene–gene edges that had primary connections to core or melanin genes, with an absolute weight greater than 0.11. The same gene–gene edges across the seven analyses were added together, and cumulative edge weights greater than 0.5 were retained. Node connectivity networks were then assembled from these using the cytoHubba plugin (Chin et al. 2014) (degree method) in Cytoscape (v3.9.1) (Shannon et al. 2003). This resulted in a network of 88 nodes and 113 edges (supplementary fig. S5, Supplementary Material online).

Supplementary Material

Supplementary material is available at *Molecular Biology and Evolution* online.

Acknowledgments

We thank Kylie Warwick for assistance with genotyping in the color locus and Cody Feuerborn, Tori Strausser, Patrick Lhomme, and Abigail Vande Veegaete for assistance in bee care or collection. Thanks to Michelle Duennes for providing *B. ephippiatus* red and black specimens for the analysis. Thanks to agencies for granting permission to collect bees, including Oregon State Parks (#270), Idaho IDFG Wildlife Research (220113), Hood River Ranger District, Montana Fish, Wildlife, and Parks, and Washington Department of Fish and Wildlife (HINES 21-321).

Funding

This project was funded by the National Science Foundation: Division of Environmental Biology, #2126417 to H.M.H., J.L., and J.B.U.K., and #1453473 (CAREER) to H.M.H.

Data Availability

All raw transcriptome sequencing data generated for *B. huntii*, *B. vosnesenskii*, *B. impatiens*, *B. bimaculatus*, and *B. melanopygus*, and whole-genome data for *B. vancouverensis*, have been deposited in the NCBI Sequence Read Archive under BioProject accession PRJNA1261059. To bolster our 0-h developmental stage comparison for *B. melanopygus*, we also retrieved and re-analyzed raw reads from the previously published BioProject PRJNA721780. Newly sequenced whole genomes for comparative *Pyrobombus* analysis are archived under BioProject accession PRJNA1237862, with sample-specific accessions available in supplementary table S3, Supplementary Material online. Metadata for each sample, as well as the custom scripts used for read preprocessing, alignment, and downstream analyses, are available in Figshare (10.6084/m9.figshare.29078816 [Referee link https://figshare.com/s/0d52776e132d7c3a777f]).

References

Andrews S. 2010. FastQC: a quality control tool for high throughput sequence data [accessed 2023 Apr 18 and 2024 Jul 3]. http://www.bioinformatics.babraham.ac.uk/projects/fastqc.

Arnoult L, Su KFY, Manoel D, Minervino C, Magriña J, Gompel N, Prud'homme B. Emergence and diversification of fly pigmentation through evolution of a gene regulatory module. *Science*. 2013:339(6126):1423–1426. https://doi.org/10.1126/science.1233749.

Auguie B, Antonov A. 2017. GridExtra: miscellaneous functions for "grid" graphics. R Package Version 2.3 [accessed 2024 Feb 16]. https://CRAN.R-project.org/package=gridExtra.

Aumer D, Stolle E, Allsopp M, Mumoki F, Pirk CW, Moritz RF. A single SNP turns a social honey bee (*Apis mellifera*) worker into a selfish parasite. *Mol Biol Evol*. 2019:36(3):516–526. https://doi.org/10.1093/molbev/msy232.

Barek H, Sugumaran M, Ito S, Wakamatsu K. Insect cuticular melanins are distinctly different from those of mammalian epidermal melanins. *Pigment Cell Melanoma Res*. 2018:31(3):384–392. https://doi.org/10.1111/pcmr.12672.

Benjamini Y, Hochberg Y. Controlling the false discovery rate: a practical and powerful approach to multiple testing. *J R Stat Soc Series B Stat Methodol*. 1995:57(1):289–300. https://doi.org/10.1111/j.2517-6161.1995.tb02031.x.

Blighe K, Rana S, Lewis M. 2018. EnhancedVolcano: Publication-ready volcano plots with enhanced colouring and labeling [accessed 2024 Nov 30]. https://github.com/kevinblighe/EnhancedVolcano.

Broad Institute. 2020. Picard Toolkit. Broad Institute, GitHub Repository [accessed 2024 Feb 8]. https://broadinstitute.github.io/picard/.

Chen S, Zhou Y, Chen Y, Gu J. Fastp: an ultra-fast all-in-one FASTQ preprocessor. *Bioinformatics*. 2018:34(17):i884–i890. https://doi.org/10.1093/bioinformatics/bty560.

Chin C, Chen S, Wu H, Ho C, Ko M, Lin C. CytoHubba: identifying hub objects and sub-networks from complex interactome. *BMC Syst Biol*. 2014:8(S4):S11. https://doi.org/10.1186/1752-0509-8-S4-S11.

Christmas MJ, Smith NM, Oldroyd BP, Webster MT. Social parasitism in the honeybee (*Apis mellifera*) is not controlled by a single SNP. *Mol Biol Evol*. 2019:36(8):1764–1767. https://doi.org/10.1093/molbev/msz100.

Crowley LM, Sivell O, Sivell D, University of Oxford and Wytham Woods Genome Acquisition Lab, Natural History Museum Genome Acquisition Lab, Darwin Tree of Life Barcoding Collective, Wellcome Sanger Institute Tree of Life Programme, Wellcome Sanger Institute Scientific Operations: DNA Pipelines Collective, Tree of Life Core Informatics Collective, Darwin Tree of Life Consortium. The genome sequence of the buff-tailed bumble bee, *Bombus terrestris* (Linnaeus, 1758). *Wellcome Open Res*. 2023:8:161. https://doi.org/10.12688/wellcomeopenres.19248.1.

Danecek P, Auton A, Abecasis G, Albers CA, Banks E, DePristo MA, Handsaker RE, Lunter G, Marth GT, Sherry ST, *et al*. The variant call format and VCFtools. *Bioinformatics*. 2011:27(15):2156–2158. https://doi.org/10.1093/bioinformatics/btr330.

Danecek P, Bonfield JK, Liddle J, Marshall J, Ohan V, Pollard MO, Whitwham A, Keane T, McCarthy SA, Davies RM, *et al*. Twelve years of SAMtools and BCFtools. *GigaScience*. 2021:10(2):giab008. https://doi.org/10.1093/gigascience/giab008.

Du X, Zhang W, Wu J, You C, Dong X. Full-length DNA sequencing provides insights into goldfish evolution under artificial selection. *Int J Mol Sci*. 2023:24(3):2735. https://doi.org/10.3390/ijms24032735.

Duennes MA, Lozier JD, Hines HM, Cameron SA. Geographical patterns of genetic divergence in the widespread Mesoamerican bumble bee *Bombus ephippiatus* (Hymenoptera: Apidae). *Mol Phyl Evol*. 2012:64(1):219–231. https://doi.org/10.1016/j.ympev.2012.03.018.

Epskamp S, Cramer AOJ, Waldorp LJ, Schmittmann VD, Borsboom D. Qgraph: network visualizations of the relationships in psychometric data. *J Stat Softw*. 2012:48(4):1–18. https://doi.org/10.18637/jss.v048.i04.

Ewels P, Magnusson M, Lundin S, Käller M. MultiQC: summarize analysis results for multiple tools and samples in a single report. *Bioinformatics*. 2016:32(19):3047–3048. https://doi.org/10.1093/bioinformatics/btw354.

Ezray BD, Wham DC, Hill CE, Hines HM. Unsupervised machine learning reveals mimicry complexes in bumblebees occur along a perceptual continuum. *Proc Biol Sci*. 2019:286(1910):20191501. https://doi.org/10.1098/rspb.2019.1501.

Ferguson LC, Green J, Surridge A, Jiggins CD. Evolution of the insect yellow gene family. *Mol Biol Evol*. 2011:28(1):257–272. https://doi.org/10.1093/molbev/msq192.

Friedman J, Hastie T, Tibshirani R. 2011. Glasso: graphical lasso: estimation of Gaussian graphical models [accessed 2024 Nov 20]. https://CRAN.R-project.org/package=glasso.

Futahashi R, Fujiwara H. Melanin-synthesis enzymes coregulate stage-specific larval cuticular markings in the swallowtail butterfly, *Papilio xuthus*. *Dev Genes Evol*. 2005:215(10):519–529. https://doi.org/10.1007/s00427-005-0014-y.

Futahashi R, Koshikawa S, Okude G, Osanai-Futahashi M. Diversity of melanin synthesis genes in insects. *Adv Insect Physiol*. 2022:62:339–376. https://doi.org/10.1016/bs.aiip.2022.03.003.

Futahashi R, Osanai-Futahashi M. Pigments in insects. In: Hashimoto H, Goda M, Futahashi R, Kelsh R, Akiyama T, editors. *Pigments, pigment cells and pigment patterns*. Singapore: Springer; 2021. p. 3–43.

Gabriel S, Celikylimaz A, Jha R, Choi Y, Gao J. GO FIGURE: a meta evaluation of factuality in summarization. In: Zong C, Xia F, Li W, Navigli R, editors. *Findings of the association for computational linguistics: ACL-IJCNLP 2021*. Association for Computational Linguistics; 2021. p. 478–487.

Galván I, Jorge A, Edelaar P, Wakamatsu K. Insects synthesize pheomelanin. *Pigment Cell Melanoma Res*. 2015:28(5):599–602. https://doi.org/10.1111/pcmr.12397.

Garaulet DL, Lai EC. Hox miRNA regulation within the *Drosophila bithorax* complex: patterning behavior. *Mech Dev*. 2015:138:151–159. https://doi.org/10.1016/j.mod.2015.08.006.

GBIF.org. 2025. GBIF Occurrence download [accessed 25 February 2025]. https://doi.org/10.15468/dl.z2ackd; https://doi.org/10.15468/dl.nu3jcv.

Ghisbain G, Lozier JD, Rahman SR, Ezray BD, Tian L, Ulmer JM, Heraghty SD, Strange JP, Rasmont P, Hines HM. Substantial genetic divergence and lack of recent gene flow support cryptic speciation in a colour polymorphic bumble bee (*Bombus bifarius*) species complex. *Syst Entomol*. 2020:45(3):635–652. https://doi.org/10.1111/syen.12419.

Gravely BR, Brooks AN, Carlson JW, Duff MO, Landolin JM, Yang L, Artieri CG, van Baren MJ, Boley N, Booth BW, *et al*. The developmental transcriptome of *Drosophila melanogaster*. *Nature*. 2011:471(7339):473–479. https://doi.org/10.1038/nature09715.

Grote S. 2024. GOfuncR: gene ontology enrichment using FUNC. R package version 1.26.0. https://doi.org/10.18129/B9.bioc.GOfuncR; [accessed 2025 Mar 26] https://bioconductor.org/packages/GOfuncR.

Heraghty SD, Jackson JM, Lozier JD. Whole genome analyses reveal weak signatures of population structure and environmentally associated local adaptation in an important North American pollinator, the bumble bee *Bombus vosnesenskii*. *Mol Ecol*. 2023:32(20):5479–5497. https://doi.org/10.1111/mec.17125.

Heraghty SD, Sutton JM, Pimsler ML, Fierst JL, Strange JP, Lozier JD. *De novo* genome assemblies for three North American bumble bee species: *Bombus bifarius*, *Bombus vancouverensis*, and *Bombus vosnesenskii*. *G3 (Bethesda)*. 2020:10(8):2585–2592. https://doi.org/10.1534/g3.120.401437.

Hines HM. Historical biogeography, divergence times, and diversification patterns of bumble bees (Hymenoptera: Apidae: *Bombus*). *Syst Biol*. 2008a:57(1):58–75. https://doi.org/10.1080/10635150801898912.

Hines HM. *Bumble bees (Apidae: Bombus) through the ages: historical biogeography and the evolution of color diversity*. Urbana, Illinois: University of Illinois at Urbana-Champaign; 2008b.

Hines HM, Kilpatrick SK, Mikó I, López-Uribe MM, Tian L. The diversity, evolution, and development of setal morphologies in bumble bees (Hymenoptera: Apidae: *Bombus* spp). *PeerJ*. 2022:10:e14555. https://doi.org/10.7717/peerj.14555.

Hines HM, Rahman SR. Evolutionary genetics in insect phenotypic radiations: the value of a comparative genomic approach. *Curr Opin Insect Sci*. 2019:36:90–95. https://doi.org/10.1016/j.cois.2019.08.013.

Hines HM, Witkowski P, Wilson JS, Wakamatsu K. Melanic variation underlies aposematic color variation in two hymenopteran mimicry systems. *PLoS One*. 2017:12(7):e0182135. https://doi.org/10.1371/journal.pone.0182135.

Hoekstra HE, Coyne JA. The locus of evolution: evo devo and the genetics of adaptation. *Evolution*. 2007:61(5):995–1016. https://doi.org/10.1111/j.1558-5646.2007.00105.x.

Jarroux J, Morillon A, Pinskaya M. History, discovery, and classification of lncRNAs. In: Rao MRS, editor. *Long non coding RNA biology*. Singapore: Springer; 2017. p. 1–46.

Jeong S, Rokas A, Carroll SB. Regulation of body pigmentation by the Abdominal-B Hox protein and its gain and loss in *Drosophila* evolution. *Cell*. 2006:125(7):1387–1399. https://doi.org/10.1016/j.cell.2006.04.043.

Kassambara A, Mundt F. 2020. Factoextra: extract and visualize the results of multivariate data analyses. R package version 1.0.7 [accessed 2024 Feb 16]. https://CRAN.R-project.org/package=factoextra.

Katoh K, Standley DM. MAFFT multiple sequence alignment software version 7: improvements in performance and usability. *Mol Biol Evol*. 2013:30(4):772–780. https://doi.org/10.1093/molbev/mst010.

Kim D, Langmead B, Salzburg SL. HISAT: a fast spliced aligner with low memory requirements. *Nat Methods*. 2015:12(4):357–360. https://doi.org/10.1038/nmeth.3317.

Klein T, Couso JP, Arias AM. Wing development and specification of dorsal cell fates in the absence of apterous in *Drosophila*. *Curr Biol*. 1998:8(7):417–421. https://doi.org/10.1016/S0960-9822(98)70162-9.

Koch JBU, Sim SB, Scheffler B, Lozier JD, Geib SM, Vogel K. Chromosome-scale genome assembly of the hunt bumble bee, *Bombus huntii* Greene, 1860, a species of agricultural interest. *G3: Genes, Genomes, Genetics*. 2024:14(10). https://doi.org/10.1093/g3journal/jkae160.

Kopp A, Duncan I, Carroll SB. Genetic control and evolution of sexually dimorphic characters in Drosophila. *Nature*. 2000:408(6812):553–559. https://doi.org/10.1038/35046017.

Kronforst MR, Barsh GS, Kopp A, Mallet J, Monteiro A, Mullen SP, Protas M, Rosenblum EB, Schneider CJ, Hoekstra HE. Unraveling the thread of nature's tapestry: the genetics of diversity and convergence in animal pigmentation. *Pigment Cell Melanoma Res*. 2012:25(4):411–433. https://doi.org/10.1111/j.1755-148X.2012.01014.x.

Kronforst MR, Papa R. The functional basis of wing patterning in *Heliconius* butterflies: the molecules behind mimicry. *Genetics*. 2015:200(1):1–19. https://doi.org/10.1534/genetics.114.172387.

Krueger F. 2015. Trim Galore! A wrapper tool around Cutadapt and FastQC to consistently apply quality and adapter trimming to FastQ files [accessed 2024 Feb 8]. http://www.bioinformatics.babraham.ac.uk/projects/trim_galore/.

Krueger F, James F, Ewels P, Afyounian E, Schuster-Boeckler B. 2021. FelixKrueger/TrimGalore: a wrapper around Cutadapt and FastQC to consistently apply adapter and quality trimming to FastQ files, with extra functionality for RRBS data. Version 0.6.7. [*Computer software*]. Zenodo. https://doi.org/10.5281/zenodo.5127899.

Langfelder P, Horvath S. WGCNA: an R package for weighted correlation network analysis. *BMC Bioinformatics*. 2008:9(1):559. https://doi.org/10.1186/1471-2105-9-559.

Lê S, Josse J, Husson F. FactoMineR: an *R* package for multivariate analysis. *J Stat Softw*. 2008:25(1):1–18. https://doi.org/10.18637/jss.v025.i01.

Li G, Chen Q, Bai Q, Feng Y, Mao K, Yang M, He L, Liu M, Liu J, Wan D. LncRNA expression analysis by comparative transcriptomics among closely related poplars and their regulatory roles in response to salt stress. *Tree Physiol*. 2023:43(7):1233–1249. https://doi.org/10.1093/treephys/tpad041.

Li H. Aligning sequence reads, clone sequences and assembly contigs with BWA-MEM. arXiv 1303.3997. https://doi.org/10.48550/arXiv.1303.3997, 16 March 2013, preprint: not peer reviewed.

Li H, Durbin R. Fast and accurate short read alignment with Burrows-Wheeler transform. *Bioinformatics*. 2009:25(14):1754–1760. https://doi.org/10.1093/bioinformatics/btp324.

Li H, Handsaker B, Wysoker A, Fennell T, Ruan J, Homer N, Marth G, Abecasis G, Durbin R. The Sequence Alignment/Map format and SAMtools. *Bioinformatics*. 2009:25(16):2078–2079. https://doi.org/10.1093/bioinformatics/btp352.

Liao Y, Smyth GK, Shi W. featureCounts: an efficient general purpose program for assigning sequence reads to genomic features. *Bioinformatics*. 2014:30(7):923–930. https://doi.org/10.1093/bioinformatics/btt656.

Lin J, Xiao D, Wu M, Chen X, Xu Q, Wang S, Zang L. Pleiotropic effects of *Ebony* on pigmentation and development in the Asian multi-colored ladybird beetle, *Harmonia axyridis* (Coleoptera: Coccinellidae). *Insect Mol Biol*. 2025:34(2):263–277. https://doi.org/10.1111/imb.12968.

Liu Y, Ramos-Womack M, Han C, Reilly P, Brackett KL, Rogers W, Williams TM, Andolfatto P, Stern DL, Rebeiz M. Changes throughout a genetic network mask the contribution of Hox gene evolution. *Curr Biol*. 2019:29(13):2157–2166.e6. https://doi.org/10.1016/j.cub.2019.05.074.

Love MI, Huber W, Anders S. Moderated estimation of fold change and dispersion for RNA-Seq data with DESeq2. *Genome Biol*. 2014:15(12):550. https://doi.org/10.1186/s13059-014-0550-8.

Lozier JD, Strange JP, Heraghty SD. Whole genome demographic models indicate divergent effective population size histories shape contemporary genetic diversity gradients in a montane bumble bee. *Ecol Evol*. 2023:13(2):e9778. https://doi.org/10.1002/ece3.9778.

Lozier JD, Strange JP, Koch JB. Landscape heterogeneity predicts gene flow in a widespread polymorphic bumble bee, *Bombus bifarius* (Hymenoptera: Apidae). *Conserv Genet*. 2013:14(5):1099–1110. https://doi.org/10.1007/s10592-013-0498-3.

Lozier JD, Strange JP, Stewart IJ, Cameron SA. Patterns of range-wide genetic variation in six North American bumble bee (Apidae: *Bombus*) Species. *Mol Ecol*. 2011:20(23):4870–4888. https://doi.org/10.1111/j.1365-294X.2011.05314.x.

Luo M, Wang L, Yin H, Zhu W, Fu J, Dong Z. Integrated analysis of long non-coding RNA and mRNA expression in different colored skin of koi carp. *BMC Genomics*. 2019:20(1):515. https://doi.org/10.1186/s12864-019-5894-8.

Martin A, Serano JM, Jarvis E, Bruce HS, Wang J, Ray S, Barker CA, O'Connell LC, Patel NH. CRISPR/Cas9 mutagenesis reveals versatile roles of Hox genes in crustacean limb specification and evolution. *Curr Biol*. 2016:26(1):14–26. https://doi.org/10.1016/j.cub.2015.11.021.

Massey JH, Wittkopp PJ. The genetic basis of pigmentation differences within and between *Drosophila* species. *Curr Top Dev Biol*. 2016:119:27–61. https://doi.org/10.1016/bs.ctdb.2016.03.004.

McKenna A, Hanna M, Banks E, Sivachenko A, Cibulskis K, Kernytsky A, Garimella K, Altshuler D, Gabriel S, Daly M, *et al*. The Genome Analysis Toolkit: a MapReduce framework for analyzing next-generation DNA sequencing data. *Genome Res*. 2010:20(9):1297–1303. https://doi.org/10.1101/gr.107524.110.

Merrill RM, Dasmahapatra KK, Davey JW, Dell'Aglio DD, Hanly JJ, Huber B, Jiggins CD, Joron M, Kozak KM, Llaurens V, *et al*. The diversification of *Heliconius* butterflies: what have we learned in 150 years? *J Evol Biol*. 2015:28(8):1417–1438. https://doi.org/10.1111/jeb.12672.

Monniaux M. Unusual suspects in flower color evolution. *Science*. 2023:379(6632):534–535. https://doi.org/10.1126/science.adg2774.

Ng M, Dia-Benjumea FJ, Cohen SM. *Nubbin* encodes a POU-domain protein required for proximal-distal patterning in the *Drosophila* wing. *Development*. 1995:121(2):589–599. https://doi.org/10.1242/dev.121.2.589.

Osanai-Futahashi M, Ohde T, Hirata J, Uchino K, Futahashi R, Tamura T, Niimi T, Sezutsu H. A visible dominant marker for insect transgenesis. *Nat Commun*. 2012:3(1):1295. https://doi.org/10.1038/ncomms2312.

Owen RE, Plowright RC. Abdominal pile color dimorphism in the bumble bee, *Bombus melanopygus*. *J Hered*. 1980:71(4):241–247. https://doi.org/10.1093/oxfordjournals.jhered.a109357.

Öztürk-Çolak A, Marygold SJ, Antonazzo G, Attrill H, Goutte-Gattat D, Jenkins VK, Matthews BB, Millburn G, dos Santos G, Tabone CJ, *et al*. FlyBase: updates to the *Drosophila* genes and genomes database. *Genetics*. 2024:227(1):iyad211. https://doi.org/10.1093/genetics/iyad211.

Page AJ, Taylor B, Delaney AJ, Soares J, Seemann T, Keane JA, Harris SR. SNP-sites: rapid efficient extraction of SNPs from multi-FASTA alignments. *Microb Genom*. 2016:2(4):e000056. https://doi.org/10.1099/mgen.0.000056.

Paria SS, Rahman SR, Adhikari K. fastman: A fast algorithm for visualizing GWAS results using Manhattan and Q-Q plots. bioRxiv 488738. https://doi.org/10.1101/2022.04.19.488738, 19 April 2022, preprint: not peer reviewed.

Paulo DF, Nguyen TN, Ward CM, Corpuz RL, Kauwe AN, Rendon P, Ruano REY, Cardoso AAS, Gouvi G, Fung E, *et al*. Functional genomics implicates ebony in the black pupae phenotype of tephritid fruit flies. *Commun Biol*. 2025:8(1):60. https://doi.org/10.1038/s42003-025-07489-y.

Plowright RC, Jay SC. On the size determination of bumble bee castes (Hymenoptera: Apidae). *Can J Zool*. 1977:55(7):1133–1138. https://doi.org/10.1139/z77-146.

Polidori C, Jorge A, Ornosa C. Eumelanin and pheomelanin are predominant pigments in bumblebee (Apidae: *Bombus*) pubescence. *PeerJ*. 2017:5:e3300. https://doi.org/10.7717/peerj.3300.

Purcell S, Neale B, Todd-Brown K, Thomas L, Ferreira MAR, Bender D, Maller J, Sklar P, de Bakker PIW, Daly MJ, *et al*. PLINK: a tool set for whole-genome association and population-based linkage analyses. *Am J Hum Genet*. 2007:81(3):559–575. https://doi.org/10.1086/519795.

Rahman SR, Terranova T, Tian L, Hines HM. Developmental transcriptomics reveals a gene network driving mimetic color variation in a bumble bee. *Genome Biol Evol*. 2021:13(6). https://doi.org/10.1093/gbe/evab080.

Rapti Z, Duennes MA, Cameron SA. Defining the colour pattern phenotype in bumble bees (*Bombus*): a new model for evo devo. *Biol J Linn Soc*. 2014:113(2):384–404. https://doi.org/10.1111/bij.12356.

Rauluseviciute I, Riudavets-Puig R, Blanc-Mathieu R, Castro-Mondragon JA, Ferenc K, Kumar V, Lemma RB, Lucas J, Chèneby J, Baranasic D, *et al*. JASPAR 2024: 20th anniversary of the open-access database of transcription factor binding profiles. *Nucleic Acids Res*. 2024:52(D1):D174–D182. https://doi.org/10.1093/nar/gkad1059.

Robinson JT, Thorvaldsdóttir H, Winckler W, Guttman M, Lander ES, Getz G, Mesirov JP. Integrative Genomics Viewer. *Nat Biotechnol*. 2011:29(1):24–26. https://doi.org/10.1038/nbt.1754.

Rogers WA, Grover S, Stringer SJ, Parks J, Rebeiz M, Williams TM. A survey of the trans-regulatory landscape for *Drosophila melanogaster* abdominal pigmentation. *Dev Biol*. 2014:385(2):417–432. https://doi.org/10.1016/j.ydbio.2013.11.013.

Rosa LP, Eimanifar A, Kimes AG, Brooks SA, Ellis JD. Attack of the dark clones the genetics of reproductive and color traits of South African honey bees (*Apis mellifera* spp.). *PLoS One*. 2021:16(12):e0260833. https://doi.org/10.1371/journal.pone.0260833.

Shannon P, Markiel A, Ozier O, Baliga NS, Wang JT, Ramage D, Amin N, Schwikowski B, Ideker T. Cytoscape: a software environment for integrated models of biomolecular interaction networks. *Genome Res*. 2003:13(11):2498–2504. https://doi.org/10.1101/gr.1239303.

Shen W, Le S, Li Y, Hu F. SeqKit: a cross-platform and ultrafast toolkit for FASTA/Q file manipulation. *PLoS One*. 2016:11(10):e0163962. https://doi.org/10.1371/journal.pone.0163962.

Signore SJ, Hayashi T, Hatini V. Odd-skipped genes and lines organize the notum anterior–posterior axis using autonomous and non-autonomous mechanisms. *Mech Dev*. 2012:129(5-8):147–161. https://doi.org/10.1016/j.mod.2012.05.001.

Stern DL. The genetic causes of convergent evolution. *Nat Rev Genet*. 2013:14(11):751–764. https://doi.org/10.1038/nrg3483.

Sugumaran M, Barek H. Critical analysis of the melanogenic pathway in insects and higher animals. *Int J Mol Sci*. 2016:17(10):1753. https://doi.org/10.3390/ijms17101753.

Tan G, Lenhard B. TFBSTools: an R/bioconductor package for transcription factor binding site analysis. *Bioinformatics*. 2016:32(10):1555–1556. https://doi.org/10.1093/bioinformatics/btw024.

Tian L, Hines HM. Morphological characterization and staging of bumble bee pupae. *PeerJ*. 2018:6:e6089. https://doi.org/10.7717/peerj.6089.

Tian L, Rahman SR, Ezray BD, Franzini L, Strange JP, Lhomme P, Hines HM. A homeotic shift late in development drives mimetic color variation in a bumble bee. *Proc Natl Acad Sci U S A*. 2019:116(24):11857–11865. https://doi.org/10.1073/pnas.1900365116.

Toth AL, Wyatt CDR, Masonbrink RE, Geist KS, Fortune R, Scott SB, Favreau E, Rehan SM, Sumner S, Gardiner MM. New genomic resources inform transcriptomic responses to heavy metal toxins in the common Eastern bumble bee Bombus impatiens. *BMC Genomics*. 2024:25(1). https://doi.org/10.1186/s12864-024-11040-4.

True JR, Haag ES. Developmental system drift and flexibility in evolutionary trajectories. *Evol Dev*. 2001:3(2):109–119. https://doi.org/10.1046/j.1525-142x.2001.003002109.x.

Van Belleghem SM, Lewis JJ, Rivera ES, Papa R. *Heliconius* butterflies: a window into the evolution and development of diversity. *Curr Opin Genet Dev*. 2021:69:72–81. https://doi.org/10.1016/j.gde.2021.01.010.

Werner T, Koshikawa S, Williams TM, Carroll SB. Generation of a novel wing colour pattern by the Wingless morphogen. *Nature*. 2010:464(7292):1143–1148. https://doi.org/10.1038/nature08896.

Wham BE, Rahman SR, Martinez-Correa M, Hines HM. Mito-nuclear discordance at a mimicry color transition zone in bumble bee *Bombus melanopygus*. *Ecol Evol*. 2021:11(24):18151–18168. https://doi.org/10.1002/ece3.8412.

Whiting JR. 2022. JimWhiting91/genotype_plot: Genotype Plot (v0.2.1). Version v0.2.1. [*Computer software*]. Zenodo. https://doi.org/10.5281/zenodo.5913504.

Wickham H. *Ggplot2: elegant graphics for data analysis*. New York: Springer; 2016.

Wickham H, François R, Henry L, Müller K, Vaughan D. 2023. Dplyr: a grammar of data manipulation. R package version 1.1.4 [accessed 2024 Nov 20]. https://github.com/tidyverse/dplyr, https://dplyr.tidyverse.org.

Wickham H, Henry L, Pedersen T, Luciani T, Decorde M, Lise V. 2024a. Svglite: an 'SVG' graphics device. R package version 2.1.3.9000 [accessed 2024 Nov 30]. https://github.com/r-lib/svglite, https://svglite.r-lib.org.

Wickham H, Hester J, Bryan J. 2024b. Readr: read rectangular text data. R package version 2.1.5 [accessed 2024 Nov 30]. https://github.com/tidyverse/readr, https://readr.tidyverse.org.

Williams P. The distribution of bumblebee colour patterns worldwide: possible significance for thermoregulation, crypsis, and warning mimicry. *Biol J Linn Soc*. 2007:92(1):97–118. https://doi.org/10.1111/j.1095-8312.2007.00878.x.

Xu X, Harvey-Samuel T, Yang J, You M, Alphey L. CRISPER/Cas9-based functional characterization of the pigmentation gene *ebony* in *Plutella xylostella*. *Insect Mol Biol*. 2021:30(6):615–623. https://doi.org/10.1111/imb.12730.

Yagound B, Dogantzis KA, Zayed A, Lim J, Broekhuyse P, Remnant EJ, Beekman M, Allsopp MH, Aamidor SE, Dim O, *et al*. A single gene causes thelytokous parthenogenesis, the defining feature of the cape honeybee *Apis mellifera capensis*. *Curr Biol*. 2020:30(12):2248–-2259.e6. https://doi.org/10.1016/j.cub.2020.04.033.

Yang W, Cui J, Chen Y, Wang C, Yin Y, Zhang W, Liu S, Sun C, Li H, Duan Y, *et al*. Genetic modification of a *Hox* locus drives mimetic color pattern variation in a highly polymorphic bumble bee. *Mol Biol Evol*. 2023:40(12):msad261. https://doi.org/10.1093/molbev/msad261.

Yassin A, Delaney EK, Reddiex AJ, Seher TD, Bastide H, Appleton NC, Lack JB, David JR, Chenoweth SF, Pool JE, *et al*. The pdm3 locus is a hotspot for recurrent evolution of female-limited color dimorphism in *Drosophila*. *Curr Biol*. 2016:26(18):2412–2422. https://doi.org/10.1016/j.cub.2016.07.016.